Miniature Free-Piston Engine Compressor

A THESIS
SUBMITTED TO THE FACULTY OF THE GRADUATE SCHOOL
OF THE UNIVERSITY OF MINNESOTA
BY

Dustin L. Johnson

IN PARTIAL FULFILLMENT OF THE REQUIREMENTS
FOR THE DEGREE OF
MASTER OF SCIENCE

David Kittelson
William Durfee

June, 2015

Acknowledgements

I would like to recognize my colleagues in the HMD Lab and the Mechanical Engineering Department at the University of Minnesota who have helped me in a number of ways.

Thank you to my advisors, William Durfee and David Kittelson, for their guidance through this project.

This research was supported by the Center for Compact and Efficient Fluid Power, an Engineering Research Center of the National Science Foundation.

Abstract

Hydrocarbon fuels have a much higher specific energy than electric batteries, and are thus a desirable power supply for portable devices. This type of power is lacking at the human scale. A reliable lightweight long lasting power supply will be an enabler for human assist devices and miniature robotics. A prototype miniature free-piston engine compressor is capable of running for a short time.

This research looked into design changes to increase the performance and reliability of a miniature free-piston engine compressor. The performance of the original prototype was measured. New pistons and cylinder liners were tested in the engine to address the combined issues of blow-by leakage and friction. The air compressor part of the device was tested independently. Two thermodynamic models of the air compressor were created.

In its original form, the free-piston prototype produced 11 W of compressed air power while operating; however, it could only run for up to 30 s before stalling. The new parts, when implemented in the engine, did not improve reliability. The engine did not run continuously because pressure could not be held in the cylinder due to blow-by leakage caused by too large of piston/cylinder clearance. When tested independently, the compressor was able to compress air up to 450 kPa (65 psi) above ambient pressure. Its power peaked when working against a pressure difference of 170 kPa (25 psi). The models of the compressor generally matched experimental results, but they did not capture all the details of compressor operation.

The reliability of the prototype engine has not been improved. It was found that machining pistons and cylinder liners and adding a coating did not make the parts precise enough to create an adequate piston/cylinder seal with low friction. A better seal is required before the project can move forward with the implementation of homogeneous charge compression ignition (HCCI). Independent testing of the air compressor provided information on its operation not available from the prototype. The compressor models will be useful for predicting performance when design changes are made. Accuracy in matching experimental results will be improved if the leakage phenomenon is captured in more detail.

Contents

List of Tables

List of Figures

Chapter 1

Introduction

Hydrocarbon fuels are one of the best energy storage means. Their high energy density allows for portability and high power output. However, for human-scale devices, electric batteries are the dominant energy supply. Although the energy conversion efficiency of fuels through combustion is much lower than the conversion of electricity, the energy available from hydrocarbons outweighs that of batteries. This is illustrated in Fig. 1.1 which compares the stored energy per kilogram in dimethyl ether fuel with lithium ion batteries. In converting the energy to compressed air, it is assumed that the overall efficiency of an electric system is 50% and that of an engine compressor is 5%. Even with a much lower conversion efficiency, the engine can provide almost three times as much energy because of the high energy content of hydrocarbon fuel.

An ankle-foot orthosis is being developed to assist with walking for people with disabilities [1]. This project at the University of Illinois is part of the Center for Compact and Efficient Fluid Power (CCEFP). The orthosis, actuated by compressed air, is designed to be worn by a person to assist in day-to-day life and must be unobtrusive. Its power source must last for hours without charging or refueling. A canister of pressurized air or carbon dioxide will not supply enough energy and is too bulky. An electrically driven air compressor would be a good option. However, to maximize runtime and available power, a hydrocarbon fuel should be utilized.

Internal combustion engines are a well-developed technology and have been widely used for over one hundred years. They work well for powering many portable machines like lawn mowers, cars, tractors, airplanes, and ships. However, they are much less

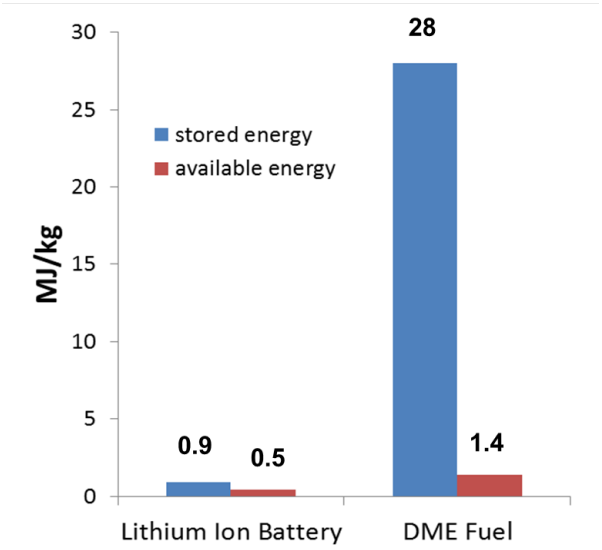

Figure 1.1: A comparison of the stored energy between lithium ion batteries and dimethyl ether fuel and the available energy if they were used to power a miniature compressor. Conversion efficiencies are assumed to be 50% for electric and 5% for fuel.

common at the miniature scale. The most widespread use of internal combustion engines in the 10-100 W range is to power model airplanes. Since this is a hobbyist industry, there has been little research on tiny engines.

One objective of this research project was to create a miniature free-piston engine and air compressor capable of powering the ankle-foot orthosis. The device should be small, lightweight, and supply 20 W of compressed air power. Another objective was to gain a better understanding of homogeneous charge compression ignition (HCCI) at the small scale. HCCI is known to be a clean, efficient combustion mode in full-size engines and will be utilized in this miniature engine.

Previous work on this research project was completed by Tian [2, 3]. Tian tested commercially available model airplane engines. He modeled their performance and validated the models through tests of an off-the-shelf engine. Tian then designed and built a prototype free-piston engine and air compressor. He did initial testing of the first running prototype. This is believed to be the world's smallest internal combustion powered air compressor.

This free-piston engine and air compressor was created to be used as the power

supply for the CCEFP ankle-foot orthosis, but there are many other areas where a compact portable supply of compressed air would be useful. This power supply could be integrated into power tools to make them more powerful and portable. Large power tools could be used in remote locations without the need for an external power source. Human-scale robots are in need of an untethered power source with extended run time. This would be an enabling technology for humanoid robots that could replace people for dangerous tasks, such as rescue and recovery missions.

There are drawbacks to the miniature engine and air compressor. All internal combustion engines produce heat and emissions along with noise and vibration. These characteristics are detrimental to a device that a person would wear throughout their daily life, as would be needed for the ankle-foot orthosis. Further research is needed to minimize these issues before the engine compressor can be used for human assist devices. Although this engine will likely never be used with the ankle-foot orthosis, there are many other possibilities for its use. Industrial applications like power tools and robotics would be more tolerant to a small amount of heat, noise, and emissions.

Chapter 2

Background

2.1 Free-Piston Engines

Internal combustion engines usually output useful power via a rotating crankshaft that is driven by one or more reciprocating pistons. In applications where the engine power is used for reciprocating motion, it makes sense to eliminate the rotating crankshaft. Free-piston engines convert the energy of a reciprocating piston directly to useful power. There are few moving parts and mechanical losses are reduced. Free-piston engines have been used for reciprocating compressors, pumps, and electric generators. For a thorough description and history of free-piston engines, see Aichlmayr's review in Chapter 2 of his PhD thesis [4] and the review by Mikalesen and Rolkilly [5].

There are three different configurations of free-piston engines. A single piston may be used where combustion occurs on one end and the load is attached to the other. The piston is driven in one direction, and some type of rebound device must return the piston to complete the cycle. The return device can be an air chamber or a mechanical spring. Second, a dual piston configuration may be used where two pistons are in line with each other facing opposite directions. The second piston acts as a rebound device for the first and the load is attached between the two. This configuration eliminates the need for a rebound device and increases the power density by having two combustion events per cycle. Third, a free-piston engine can have two opposed pistons that share a common combustion chamber. In this case, a linkage must attach both pistons to keep them in phase with one another. This configuration is similar to two single piston

engines facing each other. A rebound device is still needed to return the pistons and power can be taken of both ends of the engine. The opposed piston design has two equal masses moving in opposite directions, so it is balanced and causes much less vibration than the other designs.

Free-piston engines almost always use a two-stroke cycle where combustion occurs on every cycle. The four-stroke cycle includes an exhaust stroke and an intake stroke to exchange the burnt charge in the engine with fresh mixture. In crankshaft engines, rotational energy stored in the flywheel is used to complete this process. However, free-piston engines lack this sort of energy storage, and combustion must occur every time the piston reaches the top of its stroke in order to continue operation. Exhaust and fresh fuel-air mixture are exchanged through ports near the end of the stroke. This is scavenging, and it is an important consideration in design of any two-stroke engine.

A free-piston engine was chosen for this project because its compact design and high mechanical efficiency will be useful to power a miniature reciprocating air-compressor. A single piston configuration was chosen for its simplicity. Free-piston engines are a good match for HCCI combustion as will be further explained in Section 2.3.

2.2 Other Miniature Engine Research

This project uses a free-piston engine and homogeneous charge compression ignition (HCCI) to power an air compressor. Free-piston engines and HCCI combustion are both somewhat uncommon technologies and are especially rare at small scales.

Miniature engines have been well developed and are most commonly used in the model remote control (RC) airplane market. Because this is a hobbyist industry, they are made with basic materials and techniques in order to keep costs low. There has not been a lot of published research on miniature engines. One group that has done some work studying miniature engines is Manente, Tunestal and Johansson who began their research studying glow ignition in miniature crankshaft engines and then moved on to study HCCI [6, 7]. Glow plug ignition is the most common ignition system in miniature engines. It is similar to HCCI in that the mixture ignites when it reaches a critical pressure. The start of combustion is catalyzed by a hot platinum wire; the flame begins at this location and propagates through the combustion chamber.

Miniature engines known in the model airplane hobby as "diesels" are actually HCCI engines. Premixed fuel and air enter the cylinder and ignition is caused purely by compression with no catalyst or spark. This requires a higher compression ratio – around 15 – than glow plug ignition, which can cause harder starting especially when the engine is cold. Collair and Floweday did a thorough characterization of this type of engine [8].

Little work has been done with free-piston engines at this scale. In tiny-scale free-piston engines, HCCI is necessary for efficient combustion, as explained further in the next section. Manente, Tunestal, and Johansson have been developing the VIMPA, which is a tiny engine powered electric generator, based on their study of HCCI in miniature crankshaft engines [7]. Annen, Stickler, and Woodroffe at Aerodyne Research created free-piston engine/alternators of various sizes – 10 W, 100 W and 300 W [9]. Their engine design uses a single-ended free-piston with a return spring designed to run at the natural frequency of the spring mass system. The engine piston is attached to a linear alternator that provides electrical power. They use HCCI to minimize emissions and maximize efficiency of their engine, although prototypes use glow plug ignition.

2.3 Homogeneous Charge Compression Ignition (HCCI)

Homogeneous charge compression ignition (HCCI) is a type of low temperature combustion (LTC) that is gaining interest. It involves compression ignition, like diesel, but uses a pre-mixed homogeneous air-fuel mixture. In HCCI power output can be controlled by adjusting the mixture; therefore throttling is not necessary, eliminating associated losses. The potential for high thermal efficiency is one of the main motivations for using HCCI [10]. It has efficiency comparable to diesel, but the emissions of particulate matter and oxides of nitrogen (NO_x) are lower due to the more dilute fuel-air mixture and lower combustion temperatures [11]. It has an efficiency advantage over spark ignition due to shorter burn duration, higher compression ratio, and no throttling [11]. Manente *et al.* report that combustion efficiency of HCCI ranges from 50% - 95% from low to high load in "normal" sized engines [6]. HCCI also can be used with a wide variety of fuels including gasoline, diesel, propane, and natural gas [11]. The fuel must be easy to vaporize and easy to ignite [7].

HCCI combustion has the potential to reduce emission levels, especially of small engines. As combustion occurs in an engine, there is a boundary layer along the cool walls where the flame is quenched. Hultqvist *et al.* viewed combustion near cylinder surfaces using a tracer. They determined that reactions were slowed, but not completely quenched in a boundary layer of 1.0 - 1.5 mm, and they concluded that wall interactions are likely not the cause of high unburnt hydrocarbon emissions in HCCI engines [12].

In HCCI combustion, the air-fuel mixture is compressed until autoignition occurs. The mixture in the cylinder is compressed in a nearly adiabatic process, increasing its temperature, and creating many ignition points throughout the chamber. Locations of highest temperature ignite first, raising the pressure and temperature even further, and leading to a cascade of ignition sites. The entire mixture burns quickly without a propagating flame. The formation of autoignition sites is controlled by chemical kinetic processes that are strongly dependent on temperature, pressure, and composition. The most important chemical reaction controlling the timing of ignition is the decomposition of hydrogen peroxide (H_2O_2) [11], which is strongly temperature dependent. Optimum HCCI combustion phasing where 50% of the charge has burned is at 5-15 crank angle degrees (CAD) after top dead center (TDC) [7]. In practice, the correct phasing is difficult to achieve over a range of operating conditions. It depends on the ignition delay time, the time required for ignition to occur. Ignition delay can be controlled by varying the temperature of the air-fuel mixture (higher temperature reduces the delay) [8] and through exhaust gas recirculation [10]. Other methods include variable valve timing, variable compression ratio, and adding ozone to the intake [11]. These methods are complex and typically do not work well under transient operating conditions. A free-piston engine has a variable compression ratio, which gives it an advantage over crankshaft based HCCI engines. Without the mechanical constraint of the crankshaft, the compression ratio adjusts automatically to that required for autoignition, eliminating the need for precise timing techniques.

Correct combustion phasing is necessary for optimum performance of any combustion engine. It is easy to control timing in spark ignition engines through spark timing and diesel engines through injection timing. Since HCCI autoignition timing depends on temperature, pressure, and composition of the mixture, it is difficult to control.

However, in free-piston engines without a crankshaft, the compression ratio is not mechanically constrained and compression continues until autoignition occurs. Then the resulting gas pressure overcomes the piston inertia and piston motion reverses, so combustion is automatically centered near the effective position of TDC. If fuel, mixture ratio, temperature or other conditions change, provided that the piston has adequate inertia, the compression ratio and effective position of TDC will adjust to ensure ignition. This feature of a free-piston engine largely solves the timing problem of HCCI combustion.

The fast burn rate of HCCI is good for free-piston engines. In HCCI combustion the fuel mixture burns much faster than in conventional combustion because there is no flame propagation. In a free-piston engine the piston does not have a dwell time constrained by the crankshaft, so it responds quickly to changes in gas pressure. In fact, too quickly for a propagating flame like that in glow or spark ignition. When a propagating flame is used in a free-piston engine, combustion continues into the expansion stroke, reducing the effective expansion ratio and cycle efficiency. This effect was clearly demonstrated in this work and in earlier work by Tian [2]. The fast combustion associated with HCCI should minimize this problem.

HCCI has been known as a combustion mode for a while, but because of the challenges with ignition timing it could not be practically implemented without modern electronic sensors and controls [11]. In their 2002 paper, Epping *et al.* predicted HCCI would be implemented in the automotive industry beginning in 2010. Although it has not happened by 2015, they reported at the time that Honda already had a two-stroke one cylinder motorcycle engine that burns gasoline and uses HCCI at low to medium load [11].

Other challenges with HCCI are cold starting, operating through transient conditions, and meeting emission requirements for unburnt hydrocarbons and carbon monoxide (CO) [11]. Good operation at low and medium load has been achieved, but work is still needed for HCCI to perform well at high load and through rapid changes in load.

Fuels for HCCI

A benefit of HCCI is that a wide range of fuels can be used. Only two characteristics are necessary - the fuel must be easy to vaporize and easy to ignite. Fuels commonly used

in HCCI research in miniature engines are DME (dimethyl ether), DEE (diethyl ether), and D1000, a model airplane fuel. The addition of castor oil to D1000 for lubrication does not affect the combustion of the fuel [8]. It burns with two-stage heat realease in a Ricardo E6 test engine, but single stage heat release in a model airplane engine [8]. DEE was used by Manante *et al.* in their test. DME is being considered for this project. It typically replaces diesel fuel in conventional diesel engines larger than 500 cc per cylinder, resulting in almost no soot and slightly less NO_x but due to its low lubricity there is more wear in the injection system [13].

The current miniature free-piston prototype engine with glow plug ignition runs on model airplane fuel, which is primarily methanol and nitromethane along with some oil for lubrication. The stoichiometric air-fuel mixture for methanol is 6.47 and for nitromethane is 1.69 [14]. Raine and Thorwarth report that there is little published literature on nitromethane and that it is unknown whether or not it burns faster than methanol [14]. Nitromethane on its own is prone to pre-ignition and knocking so it is used only as a fuel additive[14]. Model airplane fuel is currently used with glow plug ignition as a stepping stone to run the prototype; it should be replaced with DME when the engine is converted to true HCCI.

In the model airplane hobby there are engines that operate with true HCCI. These engines are often called diesels, although they use a carburetor to premix the fuel. The fuel is mostly kerosene with some other ingredients to improve ignition. Lubricating oil also makes up about 20% by volume, just like regular model fuel. This model diesel fuel is not commonly available due to the rarity of these engines. Many of the hobbyists who use it mix their own formulation, so there is no standard recipe.

2.4 Small Scale Engines

There are a number of challenges associated with internal combustion engines on the small scale. As the combustion chamber is scaled down, the ratio of surface area to volume increases. Because of this, the primary challenge in small scale engines is flame quenching [15]. The propagating flame in the cylinder does not penetrate a cooler boundary layer near the metal walls. Although negligible in most full-size engines, in

small engines the volume of the boundary layer is a significant portion of the total cylinder volume. The large portion of unburnt fuel along the surfaces causes low combustion efficiency.

The purpose of a combustion engine is to convert heat to useful energy. Therefore, the properties of heat transfer are important. Since heat is lost through surfaces, the efficiency of combustion is reduced at small scales where the ratio of surface area to volume is greater. The simplest method to prevent heat from escaping would be to insulate the cylinder block. However, Manente, Tunestal, and Johansson report that this has poor results due to other effects of excessive heat on the engine [7].

Since tiny engines are used almost exclusively in the hobbyist domain, research on the subject is limited. There has been little work on exploring the potential uses of tiny engines in everyday life applications [6]. One reason for this is their environmental impacts of vibration, noise, smell, and heat [6]. Engines are often viewed in a negative light due to public opinions on fossil fuel consumption and pollution of the atmosphere. Small two-stroke engines are especially notorious for high emissions and noise, limiting interest in the possibilities of this type of power source. However, micro engines could be useful in many applications after further research to lessen their negative effects. Manente, Tunestal, and Johansson suggest an on-board power source for vehicle devices such as anti-lock brake systems or air conditioners [6]. Tiny engines will be extremely portable and would also be useful to power mobile robotics or untethered power tools. The inspiration for this project was creating an engine to power a portable human assistive device.

In the tiny volume of miniature engines, combustion is a challenge. Aichlmayr has shown experimentally that HCCI combustion is possible in a cylinder as small as 3 mm in diameter [15]. He used n-heptane as a fuel with equivalence ratios as low as 0.25, and there was no outside heating or insulation of the combustion chamber. The engine being explored in this research has a bore four times larger than Aichlmayrs test, so there is not doubt that HCCI will work.

Collair and Floweday conducted a thorough test of a small, two-stroke crankshaft engine [8]. They found that at higher engine speeds a higher compression ratio was needed for maximum power. They noted that ignition delay was shortened when pressure and temperature were increased due to higher compression ratio. The engine was

reportedly easy to start when cold, warm, or hot and ran at stable idle over 11,000 rpm. They were not able to reach the engine's rated output although they measured BMEP (brake mean effective pressure) exceeding literature values.

Hansen *et al.* also tested a small (50 cc) crankshaft engine [13]. Their engine burned DME using premixed charge ignition (PCI), which is similar to HCCI. A maximum BMEP of 309 kPa was reached at 2000 rpm and it was reported that the torque was low. The brake efficiency peaked at 22%, which was said to be comparable to a two-stroke gasoline engine. Poor scavenging, poor mixture formation, and high closed cycle heat loss were present.

A third test was conducted by Manente *et al.* who extensively studied a small (0.25 cu. in) HCCI engine, an O.S 25 model airplane engine with some modifications [6]. Optical analysis of HCCI combustion was carried out using a transparent engine head that allowed viewing of the combustion chamber during operation. The fuel used in this experiment was 80% diethyl ether (DEE) and 20% castor oil, and the fuel-air ratio was constant throughout. They found the maximum pressure rise rate was an order of magnitude less than full sized HCCI engines. The combustion speed was not affected by the crank angle degree. In some cases, second stage heat release occurred, and a third stage was even observed which was quenched by the opening exhaust port. Heat loss was less at higher speed, but friction forces became nonlinear and greatly increased. IMEP (indicated mean effective pressure) was shown to increase linearly with speed. The indicated efficiency was 13.5 times lower than normal sized HCCI engines for a number of reasons such as short circuiting, piston gap, quenching, and a boundary layer. The fuel was not completely vaporized when it entered the combustion chamber, so the temperature decreased during compression as more evaporation occurred. Because of homogeneous combustion, there was no temperature gradient in the combustion chamber while the fuel burned. Small drops of remaining liquid fuel were surrounded by a diffusion flame which led to high NO_x emissions. The temperature of homogeneous combustion was not the main cause of NO_x formation. Overall, specific emissions in this small engine were reportedly high compared to conventional HCCI engines. Hydrocarbon emissions were reportedly ten times higher than normal HCCI engines and CO values were twenty times higher than literature values. This was due to the high percentage of quenching in miniature engines. The quenching distance does not depend on engine size, but on

temperature and pressure conditions. Therefore its percentage increases as engine size decreases.

Manente *et al.* also compared the performance of the engine with a standard metal head to the optical head which has different thermal properties [6]. They showed that a head with lower thermal conductivity led to higher combustion temperatures, thus causing higher conversion efficiency. With less heat transfer there was a higher rate of pressure rise during combustion, higher maximum pressure, faster reactions, and better overall performance. These effects were even more pronounced at lower speed.

2.5 Surfaces

The interaction between the piston and cylinder surfaces is important to the performance of an engine. In the case of a tiny engine, the effects of are magnified due to the increased surface area and wider tolerances relative to the engine size. Friction and wear between sliding components must be addressed to successfully create a miniature engine.

The surface finish and the properties of the material are important. In order to minimize friction and wear, rubbing surfaces must be smooth. However, a surface finish that is too smooth can be bad – plateaus and grooves are necessary [16]. A plateaued surface created through honing holds oil in grooves to lubricate the rubbing surface of the piston. In typical engine manufacturing, a couple of honing steps are performed on the cylinder after the bore has been machined to nearly the final diameter. First, a base honing is done to create crosshatched grooves leaving peaks and valleys in the metal. Then with a softer material a second, less aggressive, honing smooths the peaks into plateaus eliminating sharp edges [17]. Honing alone is not sufficient to prevent wear [18]. Radil reports one case where honing had no effect on the wear of the tested parts, in fact he showed that honing of certain materials increased ring wear [18].

Surfaces of harder materials will wear less, but they are more prone to cause scuffing. Typically in engines the piston and cylinder are made from materials with different hardness so that most of the wear is limited to one part. Usually the piston surface is made of softer material as it is easier to replace. Therefore, the surface finish of the harder material is more critical because it acts as a file to the softer material while running [19].

Wear and scuffing are different things: wear is the gradual removal of material over many cycles, and it can actually be helpful to prevent scuffing, a rapid, drastic change in a surface. Erye says the definition of scuffing is quite variable, but gives a generally accepted definition: localized surface damage caused by solid phase welding between surfaces without localized melting [19]. Excessive heat from friction can be a major factor causing scuffing. If a high spot exists between rubbing surfaces, oil will be removed and the increased friction will cause the spot to heat up. As the material heats, it expands at the localized point, compounding the effect of the high spot [16]. Ideally, the material will wear faster than it expands eliminating the problem. However in the case of a hard material the increasing high point will not wear away and will scuff the other surface.

Scuffing usually occurs during the run-in period of a new engine [19]. During typical run-in, an adhesive wear mechanism between the piston rings and cylinder creates conforming surfaces and thus a good seal [18]. Ng *et al.* concluded that an initial burnishing, or run-in, takes about two hours [20]. Murray lists a number of factors that are likely to lead to scuffing: poor surface finish of the bore, wrong ring design, bore distortion, overheating, low lubricant viscosity, sticking rings, poor coolant flow, and carbon backing behind the rings [21].

The effect of the surface finish is even more pronounced at the small scale. The surfaces of the cylinder and piston in the miniature free-piston engine are vital to its operation. Scuffing and excessive wear caused problems [2] and must be eliminated for reliable operation of the prototype.

2.6 Coatings and Materials

Various coatings offer surface properties beyond what is possible with just machining and honing. Improved engine performance on a range of scales has been achieved through the use of coatings. Coatings are used to improve a number of properties in engine operation. Many different types of materials are used for different purposes. These include ceramics, polymers, metal plating, and diamond-like carbon (DLC). Molybdenum disulfide creates a low friction surface which reduces friction losses and wear between the piston and cylinder. Electroplated chrome and molybdenum are examined specifically by Radil for

their low friction properties [18]. He also states that the true performance of coatings cannot be gaged because engine oils are formulated specifically to work well with metal parts. When other materials are used, a specialized oil formulation likely would enhance their performance. Munro found that chromium is good for preventing ring and liner wear, and that sprayed molybdenum resists scuff, although it can increase wear on the bore [17]. Keijzers reports about using thermal spray coatings to reduce friction and wear [22]. Although his main focus was using coatings to reduce wear and friction of valves, he states that the same techniques are often used on cylinder bores and piston rings. One example that has been used for years on valve stems and piston rings is a plasma-sprayed molybdenum powder with NiCr flux. Many materials, such as molybdenum, inherently reduce friction, but the porous surface of a coating also helps hold oil so it is available to lubricate the sliding parts.

Coatings in engines are often used in the racing industry to gain performance, especially in small two-stroke engines. They seem to be most common as aftermarket additions to smaller high-performance engines, such as those used for racing motorcycles or snowmobiles. These two-stroke engines are still two orders of magnitude larger than the miniature free-piston engine of this project. Typical coatings are around 30 μm thick. When applied to a normal engine the clearance is reduced slightly, but no further modifications are needed. However, this miniature engine is so small that the thickness of the coating is greater than the tight piston/cylinder clearance. Therefore, implementing a coating in the miniature engine requires the additional complication of increasing the cylinder bore.

Ng *et al.* tested titanium and titanium carbide coatings in various configurations [20]. They compared an aluminum piston with cast iron rings, the same piston with titanium carbide (TiC) coated rings, and coating on both the piston and rings. Their cylinder was aluminum textured with honing for oil retention. With TiC coated rings, friction was reduced by 3.6%, and with coated piston and rings, it was reduced 20% from the standard set. In their test engine, 53% of total friction came from the ring-pack. They state that titanium carbide is commonly used in bearings because it has low friction and high surface hardness [20].

There are many additional considerations when using coatings to improve engine performance. In order to help coatings adhere to the base metal, carbide is added to

reduce internal stress [23]. Coatings must not delaminate; if they peel off, the benefit will be lost and it is likely that further damage will be caused to the engine. Adherence can also be improved by arranging layers in various ways [23]. Sometimes, after coatings are applied further machining may be done to improve the surface finish [18, 22]. Run-in wear may occur with ceramic coatings, but it is not always beneficial for the final surface, as it is with typical engines [18]. If the coating was designed to function optimally as applied, extra wear hinders its performance.

Coatings can also be valuable for improving thermal properties, such as reducing heat transfer. Thermal barrier coatings can be applied to the top surface of a piston, or the head of a combustion chamber. These materials, usually some type of ceramic, have a low thermal conductivity and reduce heat transfer out of the combustion chamber, which increases the thermal efficiency of an engine. In some cases, thermal barrier coatings have also been applied to exhaust systems.

Diamond-like-carbon (DLC) consists of an amorphous carbon that is used as a hard, low friction coating in many applications. It is increasingly used in engines to enhance performance. DLC first appeared in the automotive industry in 1995 [23]. DLC can be applied to pistons, cylinders, and rings, as well as liners, pins, and cams [23]. It can directly reduce friction loss by 10% [24]. DLC may be beneficial if used on the piston of the miniature free-piston engine.

Polytetrafluoroethylene (PTFE), commonly known by its brand-name, Teflon, is a durable low friction polymer. However, it does not stand up to combustion temperatures, so cannot be used in engines. PTFE can survive 250^o C intermittently, but can only tolerate 160^o C continuously in a lubricated system and 125^o C if running dry [24]. PTFE is usable either with or without lubrication, but intermittent lubrication will cause more wear. In dry running situations, a little PTFE material is rubbed off onto the opposite surface creating a film and preventing further wear. When a liquid lubricant is added, the film is washed away, and the next time the surface is dry, more material rubs off. In this way, intermittent lubrication causes high wear. If a liquid lubricant is always present, there will be little wear. PTFE is commonly used for sealing rings in air compressors but is not well suited for engines [24]. In engines a single ring holds a pressure difference too high for PTFE. Although it is not suitable for engines, the benefits of PTFE would be useful in the compressor side of the free-piston prototype.

Chapter 3

Prototype Testing and Design

A running prototype of the free-piston engine compressor was built by Tian [2] (Fig. 3.1). Both the engine and compressor were based on a piston and cylinder from a small model airplane engine – an AP Hornet 09. This is a common engine in the remote control model airplane hobby. It has a bore of 12.5 mm and a stroke of 12 mm for a displacement of 1.5 cu. cm (0.09 cu in.). The Hornet is a two-stroke engine that uses a chrome-plated brass cylinder and an aluminum piston. A piston and cylinder liner from the airplane engine were used in both the engine and the compressor of the free-piston prototype The rest of the device was mostly machined from aluminum and steel. The components of the prototype are pictured in Fig. 3.2.

Some model airplane engines, including the AP Hornet 09, have a tapered bore and negative piston/cylinder clearance at top dead center (TDC) when the engine is cold. The tight fit is overcome by the force of turning the crankshaft when starting the engine. When it warms up, thermal expansion of the cylinder creates a perfect fit between the piston and cylinder. In the free-piston configuration of the prototype, the tapered bore does not work because there is no force from the crankshaft to overcome the tight fit at TDC. When the prototype was built, the cylinder was reamed to reduce the taper and allow the piston to move freely. This is necessary for cold-starting the free-piston engine. The cylinder liner used in the compressor was also reamed to have a straight bore. Both pistons in the original prototype were unmodified. Custom reed valves were made for the air compressor. They were EDM cut from a sheet of stainless steel.

Figure 3.1: The prototype miniature free-piston engine compressor

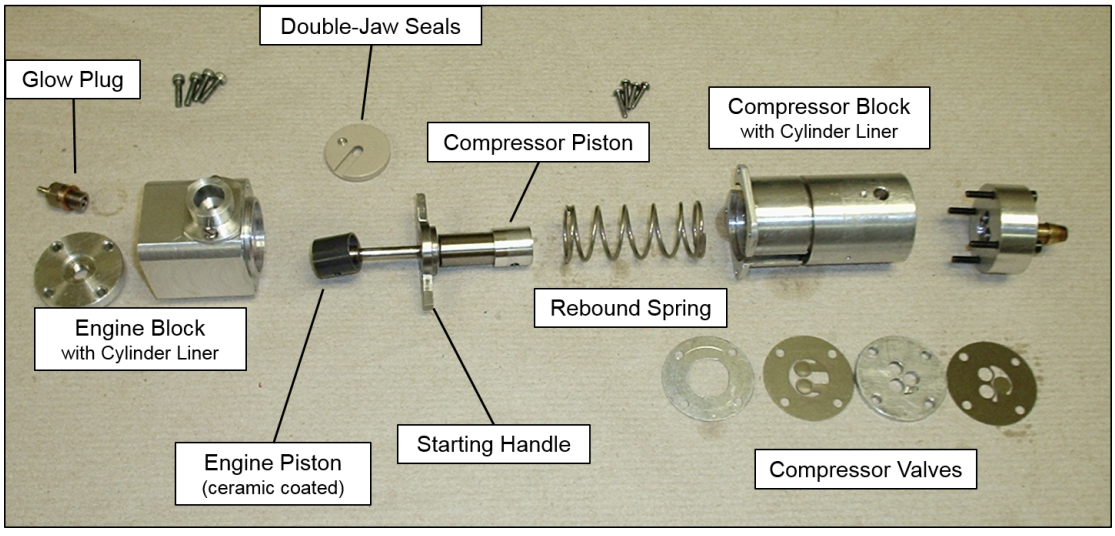

Figure 3.2: The components of the miniature free-piston engine compressor. The pistons and cylinder liners are from a model airplane engine and most of the other parts were machined from aluminum and steel.

The free-piston engine compressor uses a single power piston and a rebound spring. As combustion drives the piston down, energy is stored in the spring, which then returns the piston, causing compression for the next cycle. The air compressor piston is attached to the power piston via a connecting rod. The piston assembly also has a handle which extends from the side of the engine and is used for starting, as explained in Section 3.2.

This prototype uses a two-stroke cycle, as is common for free-piston engines. Near the bottom of the stroke, ports are uncovered to allow scavenging - exhaust exits and fresh fuel enters the cylinder. Fuel-air mixture is compressed in the sealed crankcase below the piston as it moves down, then rushes into the cylinder as the ports open. In the prototype, a custom seal was made around the piston rod with the polymer PEEK. During the upstroke of the piston, a vacuum draws in fresh fuel mixture through a reed check valve. The fuel is mixed with air in a small carburetor also taken from a stock AP Hornet 09 engine.

Through modeling and testing, Tian found that 100 Hz is the optimal operating speed to balance friction and blow-by leakage in the free-piston prototype [2]. The device was designed so that the natural resonant frequency of the spring mass system of the piston assembly is near this value. In order to accomplish this, a weight was added to the piston assembly. The spring must be strong enough to carry adequate energy from one stroke to the next for compression.

Tian's first prototype was not operable due to alignment issues, but his second design does run [2]. Since the engine is similar to a model airplane engine, model "nitro" fuel is used. In order to reach the goals of this project, a cleaner burning, more efficient fuel will need to be used, but the model airplane fuel provides the easiest way to get the prototype running. The fuel is a mixture of methanol, nitromethane, and lubricating oil. This type of methanol based fuel is available in a variety of formulations. Omega 10% by Morgan Fuels was used for all engine testing reported in this paper. This blend consists of 10% nitromethane by volume and 20% lubricating oil, which is a mixture of castor oil and synthetic oil. The balance is methanol. The fuel contains small amounts of a number of additives, but the exact formulation is a trade secret. Methanol-based fuel requires a glow plug for ignition. A platinum wire, heated by electrical resistance, catalyzes the reaction. Combustion begins and propagates through the rest of the cylinder. The current prototype engine has a stock glow plug which will be eliminated

for true homogeneous charge compression ignition (HCCI). One characteristic feature of HCCI is that there is no flame propagation during combustion. In HCCI a glow plug is not needed as the entire mixture under compression ignites almost simultaneously. This will be implemented on a future iteration of this free-piston engine, eliminating the glow plug.

Preliminary testing of the free-piston prototype engine compressor was done by Tian [2]. These tests were repeated to confirm the findings and collect more detailed data on the compressor output. Changes were made to components of the prototype with the goal of increasing run time and further tests were conducted to determine their effectiveness.

3.1 Testing Apparatus

A test stand was created for running the free-piston engine compressor prototype and measuring its performance (Fig. 3.3). The prototype was fastened vertically in an aluminum frame with the compressor outlet downward. A laser position sensor (MTI, model LTC-120-20-SA) measured the position of the piston assembly while the engine ran. The laser beam shines on the engine's starting handles which protrude from its body and move with the pistons while it runs. The combustion pressure was measured by a small pressure transducer (Optrand, model D22255-Q) mounted in the engine's head. Data from these devices were recorded by data acquisition (DAQ) software at a rate of 20 kHz.

Fuel was supplied to the engine's carburetor through stock model fuel hose. A 25 mL burette was used as the fuel reservoir. A float bowl mounted just above the carburetor maintained consistent fuel pressure as the level in the burette changed. Sometimes a simple fuel tank was used. The positioning of the fuel tank was easily changed up and down to adjust the fuel pressure.

The prototype's compressed air output was connected to a 530 mL reservoir via a hose. An inline check-valve prevented backflow leakage when the compressor was not running. The reservoir was held at a constant pressure with a backpressure regulator. The flow of air exiting through the regulator was measured by a mass flow sensor (TSI, model 41221). The reservoir pressure was measured with a pressure sensor (Omegadyn,

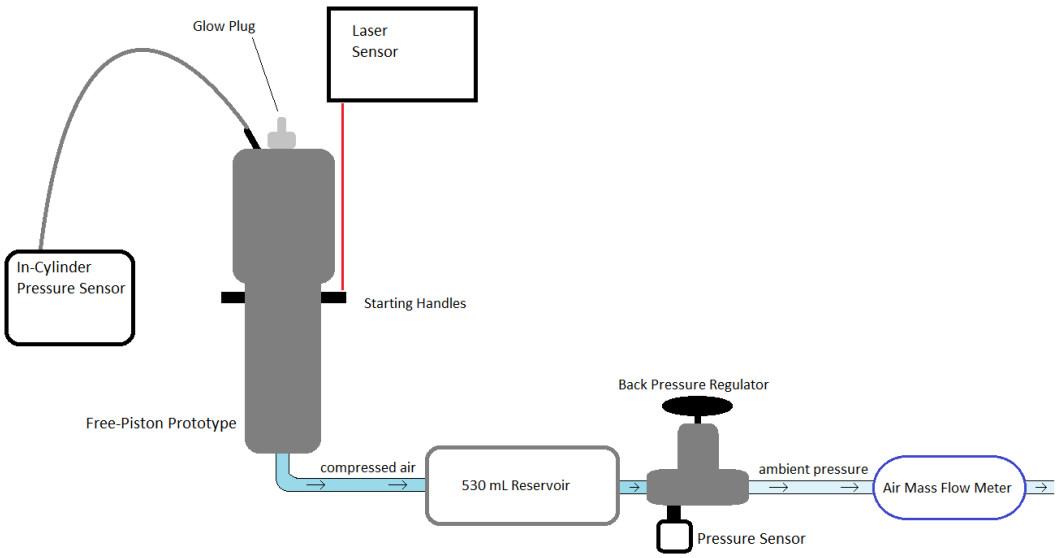

Figure 3.3: A diagram of the test stand for the free-piston prototype

model PX309-150G5V). These sensors were connected to the same DAQ and read at a rate of 100 Hz. Since the reservoir pressure was held constant, the measured mass flow of air exiting was assumed to be the same as the mass flow of air produced by the compressor. The mass flow rate and the backpressure can be used to calculate the output power of the air compressor. This data is presented at the end of Section 3.3. This system for measuring compressed air output was also used for the independent testing of the air compressor, as described in Chapter 4.

3.2 Starting the Engine

A number of steps were followed to start the miniature free-piston engine. The needle valve of the stock model airplane carburetor was opened four full turns, and the glow plug was connected to 1.5 V supplied by a pair of D batteries. Once the engine was running, combustion kept the glow plug hot and electric power could be removed. The glow plug is a platinum wire which, when hot, ignites the fuel through catalytic effects. The standard operating procedure for starting and running the prototype is given in Appendix A.

The engine was started manually as an automatic starting system has not yet been

developed. Using the handles attached to the piston assembly, the engine was cycled a few times by hand to bring fresh fuel-air mixture into the cylinder. Then the handles were pulled down all the way, compressing the rebound spring, and released. The spring pushed the piston assembly upward compressing the fuel charge and causing ignition. A pair of metal bars were used to pull down and release the handles, as it is impossible to release them cleanly with ones fingers. If combustion occurs, the piston assembly is driven down and continuous running begins. Firing must occur on every cycle to keep the free-piston engine running because there is no flywheel to hold momentum from one cycle to the next. More information about starting mechanisms is presented in Appendix B.

In testing, the starting handles had to be pulled and released many times before the engine would start. This was due to the variation in the fuel mixture provided by the carburetor. Each manual cycle brought a new fuel-air charge into the combustion chamber until one of them had the correct conditions for ignition and combustion.

3.3 Initial Prototype Test Results

The prototype free-piston engine compressor was run and its performance was measured. To begin, the prototype had its original cylinder liners, stock pistons, and glow plug ignition. Tian had run the engine for up to six minutes before it stalled [2]. The goal of the first study was to replicate previous results and collect more data from the operating device.

When the starting handles were released, the spring pushing the pistons up created compression of around 2000 kPa in the engine cylinder. This was adequate pressure to cause ignition if a good fuel-air mixture was present. Figure 3.4 shows a pressure trace and the piston position as the engine started. During continuous running the peak cylinder pressure was usually around 3000 kPa, however it took a few cycles to reach this level. Because the first cycle was weak, the piston assembly did not move down as far as during continuous running. However, to continue operating, the exhaust and intake ports must be uncovered to refresh the fuel-air mixture. Once this happened, the spring pushed the piston assembly back up at full speed beginning regular running.

The prototype free-piston engine tended to stall quickly. In these tests, it typically

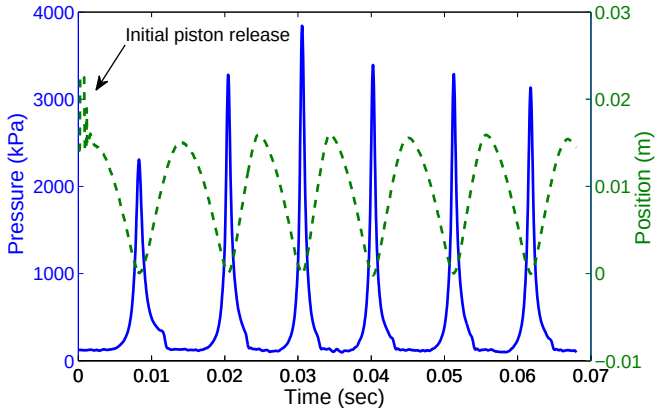

Figure 3.4: Startup behavior of the engine - pressure and position traces

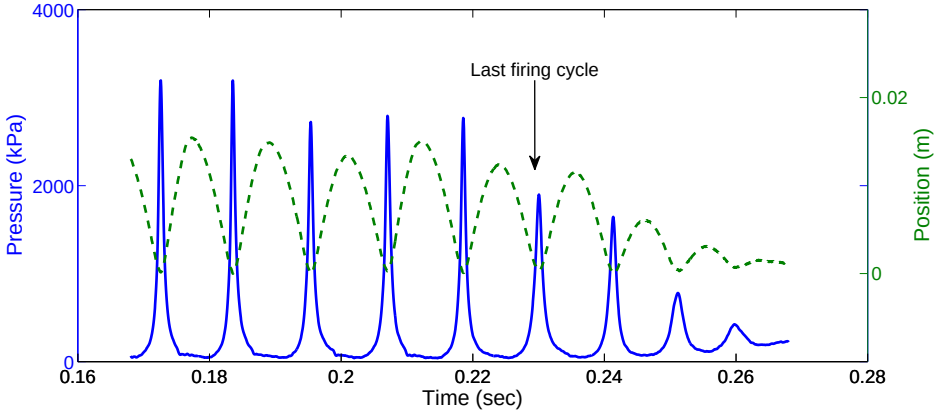

Figure 3.5: Pressure and position traces as the engine stalls

ran 20 s or less. At 100 Hz, 20 s of running is 2000 cycles. Often it stalled after less than one second of running. Figure 3.5 shows the engine stalling 0.25 s after starting. This behavior where there is a noticeable decline in pressure over the last seven to eight cycles was typical of stalling after longer runs, as well.

A number of combined factors caused the engine to stall. They include excessive friction between the piston and cylinder, blow-by leakage causing lack of compression, and inconsistent fuel-air mixture.

The prototype uses a carburetor from a model airplane engine, also the AP Hornet 09, to mix fuel with air as it enters the engine. At this small scale, the carburetor cannot

easily create a precise mixture. It is also likely that the fuel was not completely vaporized before entering the engine. These factors led to an inconsistent mixture entering the combustion chamber. Due to the nature of the free-piston engine requiring combustion on every cycle, it will stall from a single weak charge.

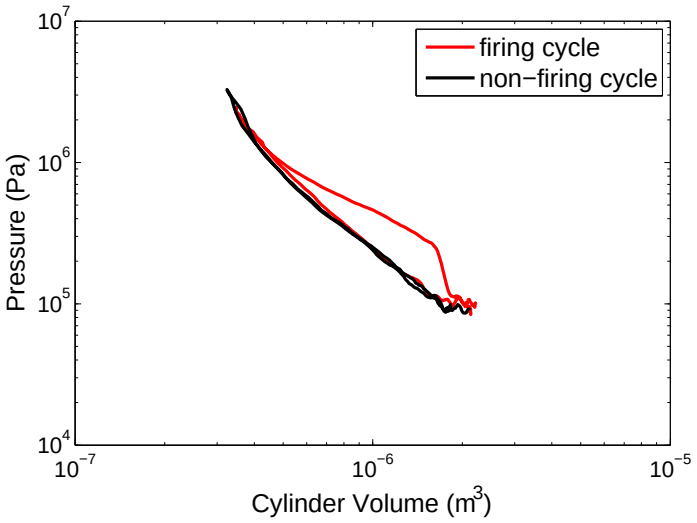

Figure 3.6: PV diagram of engine operation

Figure 3.6 shows a pressure-volume curve of the prototype engine. In the free-piston engine the curve is narrow indicating low efficiency. This is due to the rapid response of the piston to increasing pressure from combustion. There is no mechanical constraint, as a crankshaft would provide, to hold the piston at the top position while fuel burns and pressure increases. Since the prototype uses glow plug ignition it takes time for the flame to propagate through the cylinder and burn all of the mixture. While this is happening, the piston is already descending preventing pressure from building as high. With HCCI combustion, there will be no flame propagation. The fuel will burn much faster, and peak pressure will be reached before the piston retreats as far. This should greatly increase cycle efficiency.

Not only was the combustion slow, but it appears to occur relatively late in the cycle. This is evident in Fig. 3.6. The trace of the firing cycle follows the non-firing cycle through compression and continues to follow it back down the PV curve through the beginning of expansion. Finally it deviates as added pressure from combustion is

present. This late combustion can also be seen in Fig. 3.4 where the first pressure peak has a noticeable shoulder on the right side. Significant combustion occurred well after the peak preventing pressure from dropping as quickly. Although the shoulder is not as prominent, the subsequent peaks in Fig. 3.4 also show this effect where they widen near the bottom as additional combustion slowed the decline in pressure.

The noise level of the prototype was measured when it was running with a hand-held decibel meter. At a distance of one foot, the maximum noise level was 100 dB. It was not reduced when a silencer from a stock model airplane engine was used on the prototype.

Air Power Produced by the Prototype

The output power of the prototype was found by calculating the energy available from the compressed air in the reservoir. In one test, the engine ran for 18 s pressurizing the 530 mL reservoir from ambient pressure to 446 kPa (50 psig). The energy stored in the compressed air was calculated by finding the work done if expanded to ambient pressure:

$$W = n * c_v * \Delta T \ . \tag{3.1}$$

The number of moles, n, was found from the ideal gas law. It was assumed that the pressurized air in the reservoir had cooled to ambient temperature. As the air expands, the temperature would decrease farther. Assuming adiabatic expansion, the new expanded temperature of air was found as

$$T_f = T_i \left(\frac{p_f}{p_i} \right)^{1-\frac{1}{\gamma}} \tag{3.2}$$

where p_i is the reservoir pressure, p_f is ambient pressure, and T_i is ambient temperature. Using this in eqn. (3.1) it was found that $W = 205$ J. Over 18 s of operation, the average power output was 11 W. This is 55% of the project's goal of producing 20 W.

If an isothermal expansion were assumed, the initial to final volume ratio is inversely proportional to the pressure ratio and the work can be found as

$$W = p_i * V_i * ln \left(\frac{p_i}{p_f} \right) \tag{3.3}$$

where the subscript i represents initial conditions (pressurized) and the subscript f represents final conditions (expanded). The isothermal work of 530 mL of air at 446

kPa (50 psig) expanded to ambient pressure was calculated to be 350 J. Over 18 s the average power was 19 W. The actual expansion process would be somewhere between purely adiabatic and purely isothermal. Therefore the compressor's power output is bounded by 11 W and 19 W. It was likely close to 11 W, as the expansion process is nearly adiabatic.

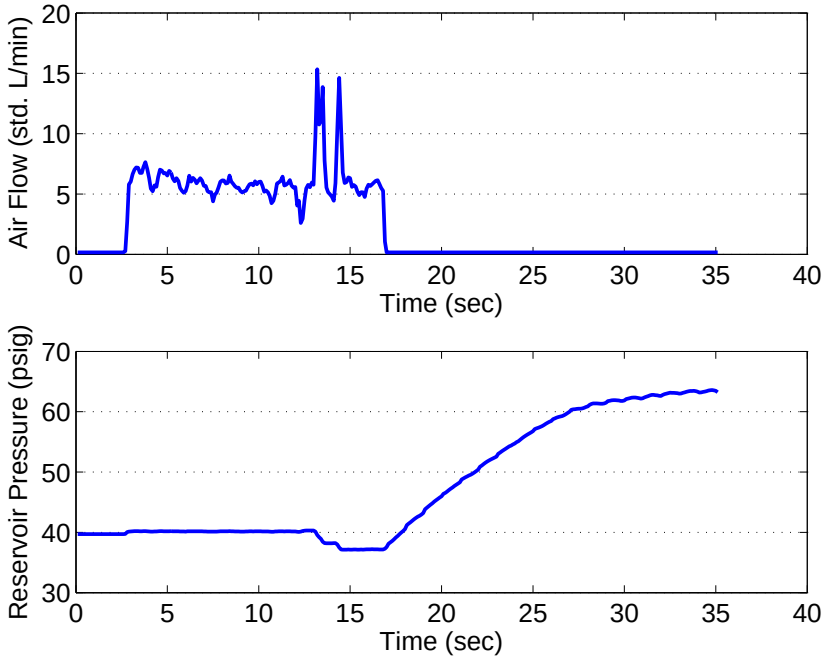

Figure 3.7: Airflow and reservoir pressure measured during a 32 s run of the free-piston prototype

In other tests of the prototype, airflow data and reservoir pressure were measured during operation. Figure 3.7 shows data from a 32 s run. The reservoir was initially pressurized to 377 kPa (40 psig). The engine was started at 2.5 s. Airflow was nearly constant at 0.12 mg/s (6 std. L/min) for the first 10 s of operation. Then the regulator was closed so that air was no longer released and the pressure of the reservoir increased. From 17 s until it stalled at 35 s, the engine compressor pressurized the reservoir, reaching 535 kPa (63 psig). The transient behavior between 13 and 17 s in Fig. 3.7 was caused by the manual adjustment of the backpressure regulator.

During steady state operation with constant pressure and flow rate, the output power can be found as

$$P = \dot{n} * c_p * T * \left[1 - \left(\frac{p_{amb}}{p_{res}}\right)^{\gamma - \frac{1}{\gamma}}\right] \tag{3.4}$$

which is derived in Section 4.2. The mole flow rate $\dot{n}$ was found from the mass flow rate, and the temperature T was assumed to be ambient. This is the power available from the compressed air leaving the reservoir after it cools to ambient pressure. The calculation should yield a similar result as the previous one, but by measuring flow rate, it allows for the calculation of instantaneous power instead of just an average. In the first part of the data shown in Fig. 3.7 at constant pressure, the power calculated in this way was 11 W, which is the same as the previously calculated average.

3.4 Design Improvements

In the prototype engine, the piston and cylinder liner were from a stock model airplane engine, an AP Hornet 09 [2]. The piston is aluminum and the cylinder liner is brass with chrome plating. In the off-the-shelf engine configuration, there is negative clearance at top dead center (TDC) at ambient temperature. This makes the airplane engine difficult to turn over when cold, but the clearance evens out as the parts heat up, creating free movement with a good seal. Extra force provided by the crankshaft is required to turn over the cold engine. In the free-piston configuration with no crankshaft, the rebound spring does not provide enough force to overcome the tight fit. Therefore the cylinder liner was reamed from 12.48 mm at TCD to 12.51 mm [2]. This allowed for free movement in the cold engine, but led to increased clearance and excessive blow-by leakage when the parts warmed up and expanded. Due to surface defects from extra machining, scuffing and increased wear were observed in the modified piston and cylinder liner, contributing to limited runtime [2].

The main barrier limiting the runtime of the current prototype is the precision of the piston/cylinder interaction. Although model airplane engines operate reliably, they are made to be inexpensive for hobbyists to purchase. Therefore they use common materials and simple processes in manufacturing. The miniature free-piston engine cannot tolerate

as much variability in machining, and higher precision components are required for it to operate well.

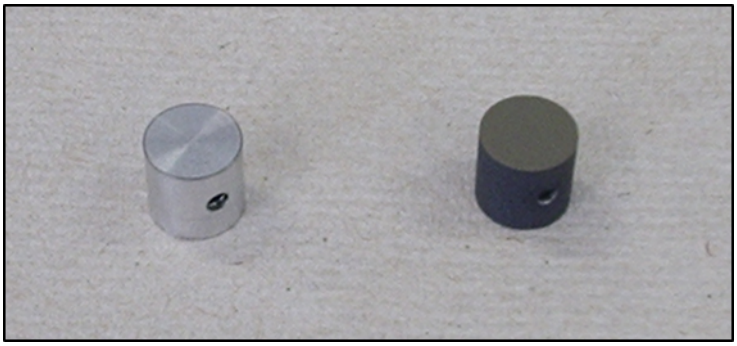

Figure 3.8: A stock piston (left) compared to a piston with a low friction coating (right)

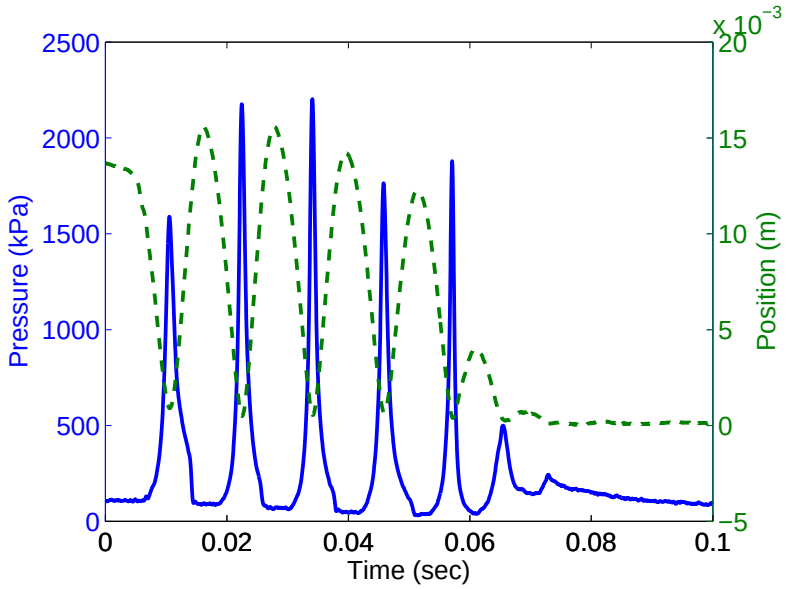

Figure 3.9: Pressure and position from testing a coated piston

The first attempt to improve the piston/cylinder interaction was to apply a commercially available dry lubricant coating to the stock aluminum piston. This treatment is often done to improve the performance of small two-stroke engines for racing snowmobiles or motorcycles. The coating (Fig. 3.8) was applied to the sides of the engine piston to reduce friction. It also is a hard material which should reduce the wear rate,

allowing the parts to last longer. The commercially applied coating was 30 μm thick, so the bore of the cylinder liner needed to be increased to allow free movement of the larger diameter piston. The cylinder liner was reamed further to 12.56 mm and honed. This cut almost all the way through the chrome plating. With the coated piston installed, the prototype free-piston engine would not run. It would fire once upon initial compression, but continuous running was never achieved. An example of data from these tests is shown in Fig. 3.9.

To diagnose the problem with the modified piston and cylinder liner, detailed measurements were made, and the dimensions of the modified parts were compared to the previous operable configuration. The piston and cylinder liner were measured with a roundness tester (Mitutotyo, model RA-2200AH). The original aluminum piston had cylindricity of $7.8 \pm 1.0 \mu m$ ($306 \pm 40 \mu$in.) and the coated piston had cylindricity of $12.2 \pm 1.0 \mu m$ ($480 \pm 40 \mu$in.). The original cylinder liner had cylindricity of $10.6 \pm 1.0 \mu m$ ($416 \pm 40 \mu$in.) and the enlarged cylinder liner had cylindricity of $55.7 \pm 1.0 \mu m$ ($2194 \pm 40 \mu$in.). The coating added variation to the surface of the piston, and the larger diameter cylinder liner had been deformed by extra reaming. The modified parts caused an irregular piston/cylinder clearance in the engine. Although the coating was intended to reduce friction, high points on the surfaces increased friction while low points widened the gap leading to more leakage. The inconsistent surfaces increased the problems with both friction and blow-by leakage.

The average diameter of the pistons and cylinder liners were measured with a coordinate measuring machine (CMM) (Global Advantage, model 7107). These results are summarized in Tab. 3.1. In the original piston/cylinder combination, the average clearance was 10.2 μm (0.0004 in.) and in the modified parts it was 7.6 μm (0.0003 in.). The average clearance was not considerably different; the engine operation was affected more by the irregular surfaces.

In the ANSI B4.1 standard for running clearances (RC), the piston/cylinder clearance of less than 15 μm (0.006 in.) is in the range of class RC1 and RC2. The ANSI standard says that for free running, the clearance should be in class RC3 with a range of 15 - 43 μm (0.0006 - 0.0017 in.). For applications where there is a significant temperature change, as in the engine it should be in class RC4, a clearance range of 15 - 58 μm (0.0006-0.0023 in.). To maintain a good seal, the clearance should be as small

as possible while allowing free movement and tolerating the temperature changes of the engine.

In making improved engine components, higher precision of the surface was needed. New pistons and cylinder liners were ordered from a custom fabricator. Cylinder liners were designed with a straight bore with an inside diameter of 12.55 mm (0.4940 in.) to fit the coated stock pistons with a clearance of 0.020 mm (0.0008 in.). The stock cylinder liners were brass, so new ones were made with the same metal also finished with a chrome plating. Since aluminum pistons are used, an aluminum cylinder liner was also fabricated and tested in hopes that the thermal expansion rate would match the piston preventing a change in clearance. All cylinder liners had a plating, either chrome, or low friction nickel-Teflon. New pistons were also fabricated. They had an outside diameter of 12.53 mm (0.4935 in.) so that they would run in the cylinder with a clearance of 0.012 mm (0.0005 in.). Table 3.1 gives a summary of the dimensions of all pistons and cylinder liners. The pistons were aluminum, similar to the original. All of the pistons were coated with the same nickel-Teflon used on half of the cylinder liners. Some of the custom machined parts can be seen in Fig. 3.10.

Figure 3.10: Various pistons and cylinder liners. Top, left to right: brass liner with nickel-Teflon coating, aluminum liner with chrome plating, brass liner with chrome plating. Bottom, left to right: aluminum piston with nickel-Teflon coating, stock aluminum piston with commercial low friction coating.

Cylinder Liners	I.D. (mm)	Pistons	O.D. (mm)	Clearance
Original - stock reamed	12.51	Stock	12.50	0.0102
Stock enlarged further	12.53	Stock with coating	12.53	0.0076
Custom Fabricated	12.55	Custom Fabricated	12.53	0.0127

Table 3.1: The diameters of the pistons and cylinder liners tested in this work. The custom fabricated dimensions are manufacturing specifications while the others dimensions are listed as measured. This table is repeated in Appendix D with units of inches.

3.5 Testing the Improved Prototype

The new pistons and cylinder liners have a variety of materials and coatings as discussed in the previous section and seen in Fig. 3.10. Therefore, many combinations were available to test. Not all of the possible combinations were tried as some common trends were observed. Table 3.2 summarizes the new parts that were tested and the results.

With each piston and cylinder liner installed in the engine, the starting procedure was carried out as before. When the handles were released, the piston assembly was pushed up by the spring, causing compression. If a pressure peak of around 2000 kPa was reached, firing could occur. In testing with a brass nickel-Teflon coated liner and an aluminum nickel-Teflon coated piston, peak pressure only reached 1300 kPa (Fig. 3.11). Excessive clearance caused too much leakage, so firing never occurred. Because pressure did not build, there was almost no rebound motion of the piston assembly. The work done on the piston by the pressure was calculated by integrating the area under the pressure curve during the piston's downstroke. In this case with a high amount of leakage, the work was much less than with the original parts. In a non-firing cycle with no friction or leakage loss, the pressure should push the piston back down performing equal work as the spring did moving it up. Typically, the work done by the spring pushing the piston up was in the range of 0.6 - 0.7 J. The downstroke had 0.4 - 0.5 J when the original running parts were installed (non-firing cycle). If the work was significantly less than this, pressure was lost to leakage. Otherwise friction must have been the problem, especially if the piston did not move as far. In this case, the work during the downstroke was less than 0.1 J as there was hardly any rebound.

With a brass chrome plated liner and an aluminum nickel-Teflon coated piston,

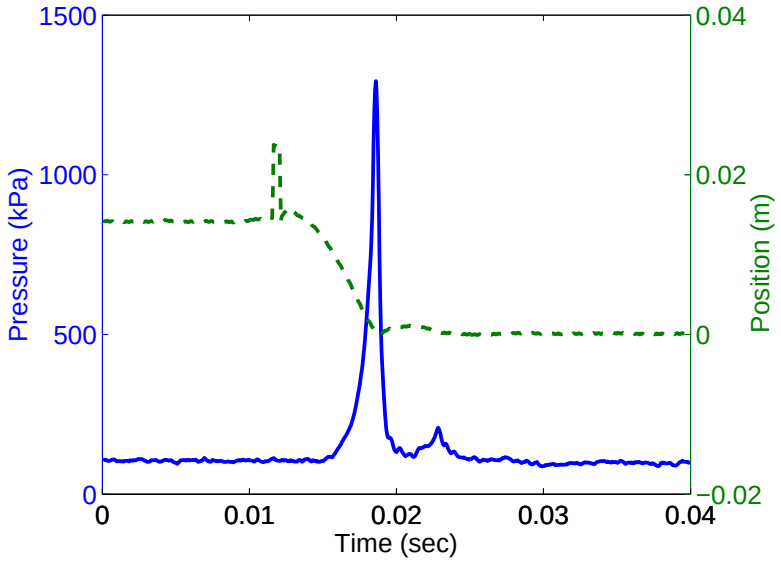

Figure 3.11: Pressure and position data from testing a brass liner with nickel-Teflon coating and an aluminum piston with nickel-Teflon coating. Peak pressure was low and there was no rebound action due to leakage.

peak pressures around 2000 kPa were reached and singular firing events were seen. An example of these data are plotted in Fig. 3.12. It is unknown if the primary problem preventing running was friction or leakage. The work on the piston during the downstroke was near the 0.4 - 0.5 J range. The piston seemed to move freely and complete the stroke, yet there was no continuous operation.

When an aluminum chrome plated cylinder liner and an aluminum nickel-Teflon coated piston were used, peak pressure reached over 2000 kPa, but no firing was observed. The work done during the downstroke was only around 0.1 J, so leakage was believed to be the problem. As the mixture rapidly leaked from the cylinder, the piston encountered less resistance and moved faster, still compressing the mixture to 2000 kPa. The peak pressure likely was not sustained long enough to begin ignition.

In these tests with the new cylinder liners and new pistons, there was too much leakage for the engine to operate. In all cases the clearance seemed to be too large to create a good seal. When selecting pistons and liners for testing, they were fit together by hand to find the best combinations. Since continuous engine operation was not

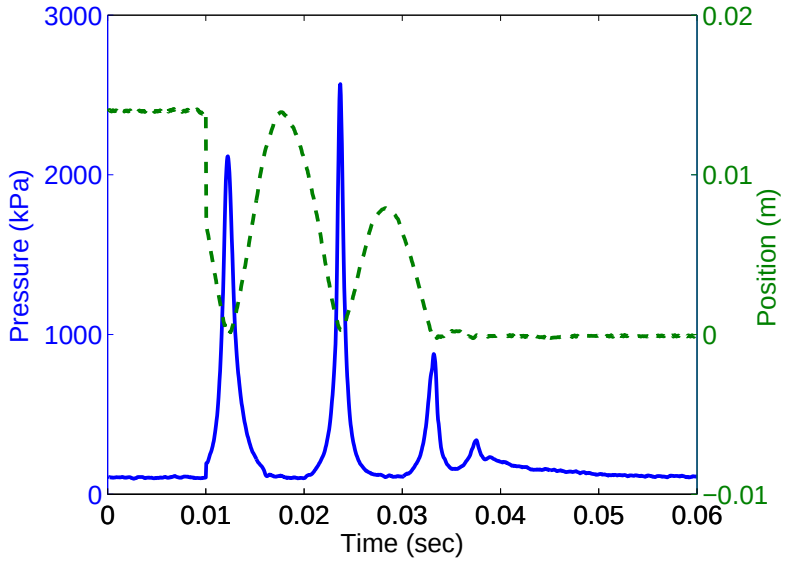

Figure 3.12: Pressure and position data from testing a brass liner with chrome plating and an aluminum piston with nickel-Teflon coating. One firing event occurred.

achieved and the engine did not warm up from combustion, the thermal characteristics of the different materials could not be compared.

The newly fabricated cylinder liners were designed so that their bore would match up with the diameter of the commercially coated stock pistons tested previously and described in the previous section. The newly fabricated cylinder liners were expected to have a much more consistent bore than the one that was initially reamed to fit the coated piston. Testing was performed with the coated stock pistons in the new cylinder liners. With a brass nickel-Teflon coated cylinder liner and the old coated piston, the maximum pressure peak was just over 1200 kPa and no firing occurred. The best combination of new parts was a custom fabricated brass chrome plated cylinder liner and a coated stock piston. When the engine was outfitted with this combination, the feel of the moving piston was the closest to the original parts. It seemed to move smoothly with little friction, yet noticeable compression could be felt. After a number of starting attempts, some wear was observed in the coating on the piston. This indicated that the surface was conforming to the cylinder. There were no large scuff marks or scratches that would hinder operation. The conformed surface should have worn down any points

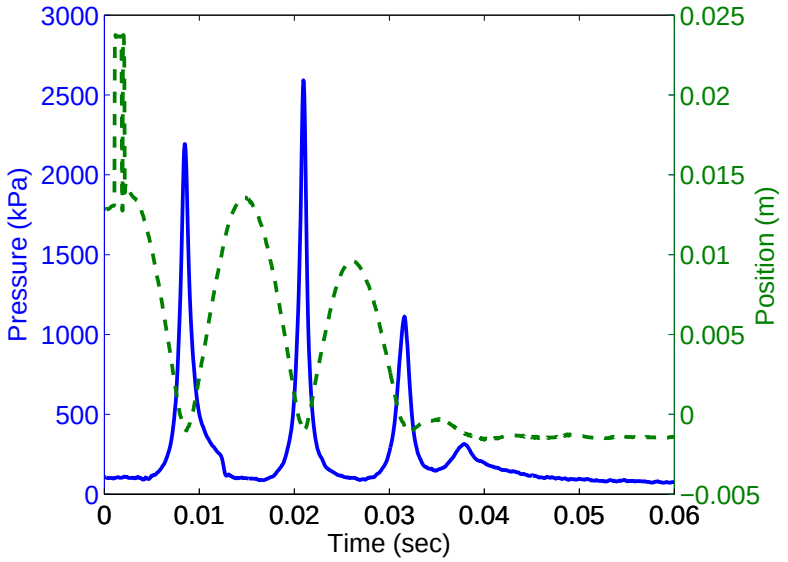

Figure 3.13: Pressure and position data from testing brass liner with chrome plating and a stock piston with a commercial low-friction coating. One firing event occurred.

that cause excessive friction, and it should fit tight enough to seal well. When starting was attempted, the engine would consistently fire on the first cycle after releasing the handles, but it never continued running. An example of data from this test is plotted in Fig. 3.13.

From these tests it was determined that blow-by leakage is most likely the main problem preventing the engine from running continuously with any of the new parts. None of the new components worked as well as the original piston and cylinder liner in the prototype.

	Piston →	Aluminum		Stock Aluminum	
Cylinder ↓	coating ↓→	Nickel-Teflon		Commercial low-friction	
Brass	Nickel-Teflon	leakage	1300	leakage	1200
Brass	Chrome	single firing	2100	single firing	2200
Aluminum	Chrome	leakage	2000	(not tested)	

Table 3.2: A summary of the pistons and cylinder liners that were tested and the results. Each listed number is the peak pressure in kPa of the first peak.

3.6 Other Prototype Engine Tests

3.6.1 Forced Air Induction

When miniature engines are used on model airplanes, the air intake of the carburetor is usually directly in the airflow path of the propeller. Therefore the engine has more efficient air induction and is essentially supercharged. The prototype free-piston engine is similar to this type of airplane engine, but does not have forced air induction. It is possible that without pressurized airflow, scavenging does not provide sufficient fuel charge to keep the engine running as it heats up.

A test of the prototype was performed to determine the effect of forced air induction. An air hose was connected from the prototype compressor outlet to the carburetor's air intake. As soon as the engine compressor began operating, airflow from the compressor was directed to the engine, providing the same effect as a spinning propeller directly in front of the intake. The pressurized air in the carburetor would tend to prevent fuel delivery and push the liquid back through the line. Therefore, a connection was made from the air line to the fuel tank so that the fuel system would be at equal pressure as the air intake.

The prototype was run, and no noticeable improvements were caused by forced air induction. The engine ran for up to 20 s and stalled. It appears that improving scavenging in this way does not prevent the engine from stalling. However, it did seem like the engine was easier to start during testing. In the first few cycles of operation, the air forced through the carburetor likely did a better job of vaporizing the fuel. In a normal startup there may be a slight delay between the first cycle and the acceleration of the incoming air, which was eliminated by supercharging.

3.6.2 True HCCI

The current free-piston prototype engine has run for short durations using nitromethane fuel and glow ignition. There is flame propagation associated with glow ignition which is not desired in this free-piston engine. Homogeneous charge compression ignition (HCCI) will provide faster, almost instantaneous combustion.

In the model airplane hobby, glow ignition is the most common type of ignition. However, there are engines that use pure HCCI combustion. They are often referred to,

incorrectly, as diesels. These engines use a carbureted fuel mixture with pure compression ignition involving no spark or catalyst. The fuel is kerosene-based with ingredients to help vaporization and lubrication. Pure HCCI requires higher compression than glow plug ignition.

True HCCI testing of the prototype was done using model "diesel" fuel from Davis Diesel. The formula of the fuel was not available from the company, but it was labeled as containing ether and petroleum distillate. To eliminate the glow plug, a special head for the engine was fabricated from aluminum. It had a flat combustion chamber. The engine piston was free to move up until it contacted the head, causing a high geometric compression ratio. In testing, the effective compression ratio only reached 8.8 due to leakage. In order to help ignite the fuel at lower compression, the engine head was heated prior to starting. An electric heat gun was used to heat the engine to 100^o C. Starting was attempted at needle valve settings ranging from 2 to 6 full turns open. No firing was detected. It is likely that even with the added heat, a compression ratio higher than 8.8 is required for compression ignition of the fuel.

3.7 Further Design Considerations

After tests of the prototype and some design changes, the reliability of the engine has not been increased. Limited runtime is the main barrier to the success of this engine. The problem is mostly related to the piston/cylinder interaction. Thermal expansion likely plays a role, as well. Further design improvements are needed to increase the reliability of the engine.

A good seal in the engine is important to minimize blow-by leakage, and the piston fit in the cylinder must allow free movement. As the engine changes temperature, a good fit must be maintained. From the testing and design changes described in this chapter, it is apparent that standard machining techniques along with coatings are not precise enough for this small scale engine. To confirm this, the custom fabricated parts should be measured with high accuracy and a comparison made to operable components. If coatings are used for thermal properties or low friction, it may be necessary to perform a final process to finish the surface after the coating is applied. Otherwise high points remaining on the surface will cause excessive friction.

In the manufacture of model airplane engines at this small scale, lapping is commonly used to create pistons and cylinder liners with the correct clearance. Then each piston and liner pair must be used together to ensure a perfect fit. It may be beneficial to explore this procedure for use in fabricating similar parts for the free-piston prototype engine.

Precision rod is available with outer diameters held to tight tolerances. This may be useful for creating a piston for the engine. A corresponding liner could be made from a bushing with a precise inner diameter. These parts could provide an accurate clearance and consistent surface. However, coatings likely would not be used as they would negate the tight tolerances of the parts' surfaces. The available sizes and materials of precision rod and bushings might be limited, as well.

Full-sized engines use piston rings to achieve a good seal between the piston and cylinder. It is rare that miniature engines use piston rings due to the complexity and resulting expense of fabrication on the small scale. Often made of cast iron, they fit loosely into groves in the side of the piston. The pressure differential forces the rings outwards against the cylinder, preventing gases from flowing past without the need for a precise piston cylinder clearance. Although they would be difficult to implement, piston rings likely would be beneficial if used in the miniature free-piston engine.

There are other features that could also be changed to improve the performance of the device. The compressor side would benefit from improved piston cylinder seal, and improvements could be made to the reed valves. When it runs for an extended time, the engine will need some sort of cooling system. This could be as simple as fins added to the block and head, or as complex as circulating a cooling fluid. The shape of the combustion chamber could be optimized by re-designing the head as long as high enough compression ratio is maintained. When different fuels are used without oil, a lubrication system will be needed for the engine; this is discussed further in Appendix C. Eventually, the engine compressor should be packaged into a self-contained power unit. It will then need an automatic starting mechanism (see Appendix B) and a control system.

Chapter 4

Testing of the Air Compressor

It is difficult to thoroughly measure the performance of the air compressor part of the prototype because the free-piston engine does not operate continuously. Independent testing of the air compressor was carried out with the purpose of understanding how well it works. This information can serve as a baseline for making future improvements and will allow for design improvement of the compressor to move forward in parallel with the work on the engine side. Continuous operation in the engine will not have to be first achieved to gage improvements made to the air compressor.

4.1 Apparatus

To collect data on the air compressor, a test stand (Fig. 4.1) was built to run the compressor with an electric motor and collect data. The test stand was made out of the engine block of the AP Hornet 09 model airplane engine. The crankshaft was spun with a belt from a variable speed electric motor and was used to reciprocate the compressor piston. Since the prototype compressor uses a cylinder liner and piston from the AP Hornet 09 engine, those components were moved from the prototype to the engine block of the test stand. The prototype check valves from the free-piston device were bolted onto the engine block in place of the original head. Output air from the compressor was sent to a 530 mL reservoir whose pressure was held constant by a backpressure regulator and measured by a pressure sensor (Omegadyne, model PX309-150G5V). An inline check valve prevented pressurized air in the reservoir from leaking

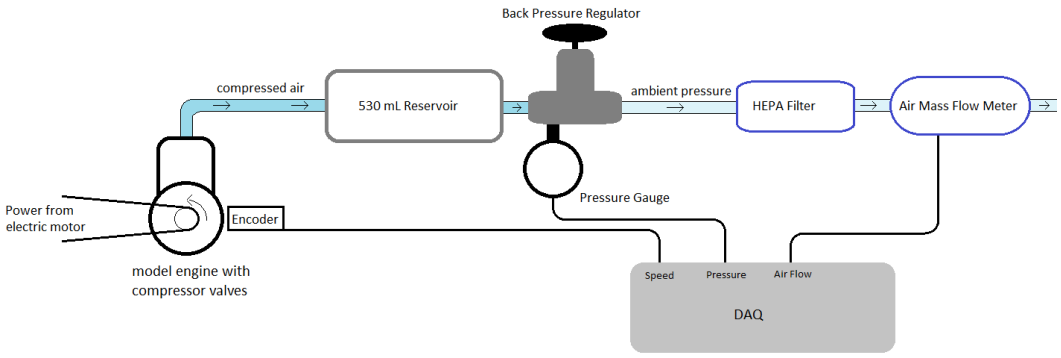

Figure 4.1: The test stand used for collecting data from the air compressor

back to the compressor. The output of the regulator at ambient pressure was piped through a low pressure-drop filter to a flow meter (TSI, model 41221). At steady state operating conditions, it was assumed that the mass flow rate of air measured exiting the reservoir was equal to the mass flow rate produced by the compressor. The flow meter, the pressure transducer, and an encoder on the crankshaft were connected to the data acquisition system.

The piston in the compressor test stand follows a slider-crank trajectory since it is run by a crankshaft. This differs from the free-piston configuration. The variable stroke of the free-piston compressor on a given cycle may be longer or shorter than the crankshaft-constrained stroke of the test stand, but it was designed to to be 12 mm on average, which is the same as the crankshaft in the test stand. For the purpose of this testing, it was assumed they are similar enough to neglect any differences in measured results.

4.2 Initial Results

During testing, data were recorded at steady state operation. The compressor was run continuously at a constant speed with the regulator set to hold the reservoir at a constant pressure, and the mass flow of air was measured (Fig. 4.2). This was repeated for different compressor speeds and a range of pressures.

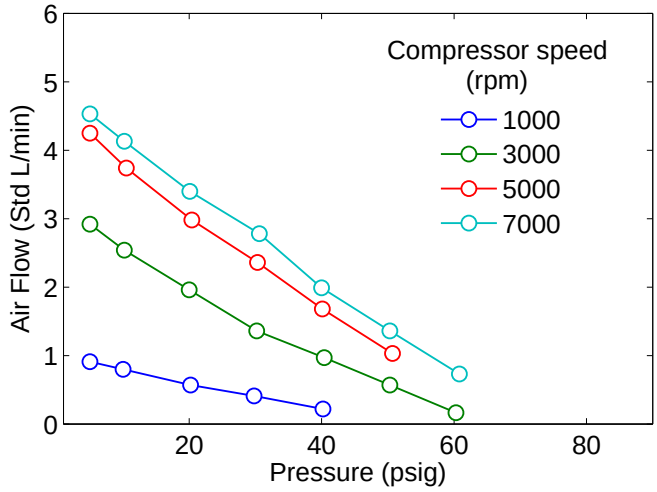

Figure 4.2: Measured airflow over a range of pressures and speeds

With knowledge of the pressure and airflow, it was possible to calculate the power available from the compressed air in the reservoir. The power was calculated as

$$P = \dot{n} * c_p(T_1 - T_2) \ . \tag{4.1}$$

P is power, $\dot{n}$ is the mole flow rate of air, the molar c_p is a constant, and T_1 and T_2 are the temperature of the compressed air and expanded air respectively. The temperature of the compressed air in the reservoir is unknown. With no heat loss, it would be the same as the compressor output, but with heat loss, it may be as low as ambient. Assuming adiabatic expansion, T_2 can be found from the pressure ratio and the temperature of the reservoir giving

$$P = \dot{n} * c_p \left[T_{res} - T_{res} \left(\frac{p_{amb}}{p_{res}} \right)^{\frac{\gamma-1}{\gamma}} \right] \ . \tag{4.2}$$

The mole flow rate can be replaced by the mass flow rate times the molar mass of air, $\dot{m} * M$. Simplifying gives

$$P = \dot{m} * M * c_p * T_{res} \left[1 - \left(\frac{p_{amb}}{p_{res}} \right)^{\frac{\gamma-1}{\gamma}} \right] \ . \tag{4.3}$$

The calculated power from the airflow data is shown in Fig. 4.3. It was assumed that the reservoir was at ambient temperature. The output power peaks when the reservoir

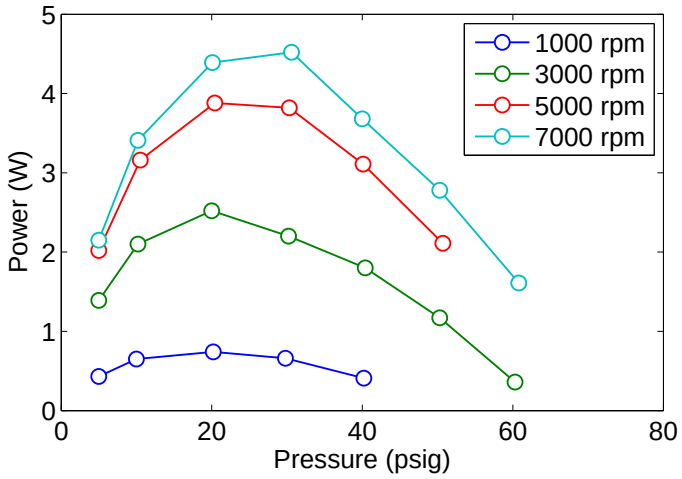

Figure 4.3: Power of compressed air output over a range of reservoir pressures calculated from experimental airflow using eqn. (4.3)

pressure is between 150 and 200 kPa gage pressure (20 and 30 psig). The input power used to run the compressor was not measured, so no conclusions can be drawn on overall efficiency.

A significant difference between running the compressor in the test stand compared to the free-piston prototype is the presence of oil. When the prototype engine is running, lubricating oil is brought in with the fuel. Excess oil is spread throughout the moving parts, including the compressor side. The presence of oil between the piston and cylinder helps seal the gap, lessening the leakage flow of air. In the compressor test stand, there was no addition of oil during operation.

A test was performed to see how much the presence of oil increased compressor output. With the compressor running at a constant 6000 rpm, the reservoir was pressurized from ambient. One test was run without extra oil in the compressor (it had some residual oil for lubrication). Then the same test was repeated, but mineral oil was slowly dripped into the air intake valve. These results are plotted in Fig. 4.4. With oil to improve the seal, 500 kPa (60 psig) was reached 17 s sooner. The maximum pressure was 632 kPa (77 psig) after 200 s of running, 69 kPa (10 psi) higher than 563 kPa (67 psig) without oil.

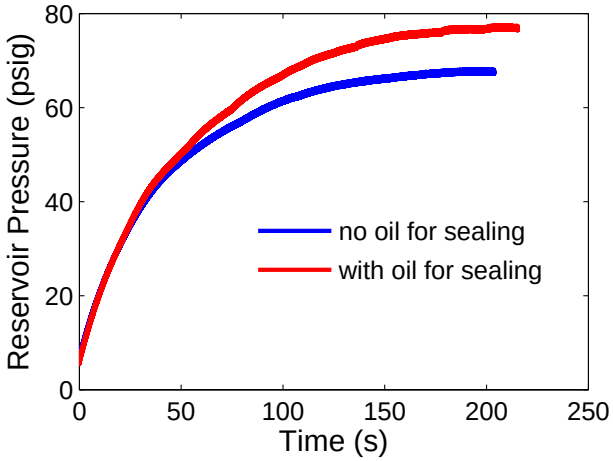

Figure 4.4: When oil is present between the piston and cylinder, it improves the seal allowing more air output from the compressor.

4.3 Modifications and Further Results

The first prototype compressor used a cylinder liner from an AP Hornet 09 engine. The ports are uncovered near the bottom of the stroke, exposing the cylinder to ambient pressure. Ideally, all air should enter and exit the cylinder through the compressor check valves. When new cylinders and pistons were custom fabricated for the engine side of the prototype, a special cylinder liner was also made for the compressor. It was dimensionally identical to the engine liner, but there were no ports. When used in the compressor test stand, it was expected that the new cylinder liner would provide greater airflow, since without ports, the full stroke could be used to compress air. A new piston was used that corresponds to the new liner. A sample of the data collected are plotted in Fig. 4.5. The new piston and cylinder combination did not seem to have as good of seal as the original prototype. Therefore, the airflow was not significantly higher. The improvement from eliminating the ports was offset by the increased gap leakage.

4.4 Conclusions from Compressor Testing

The compressor was run separately from the free-piston prototype, and the performance was measured over a range of operating conditions. The airflow data collected from the

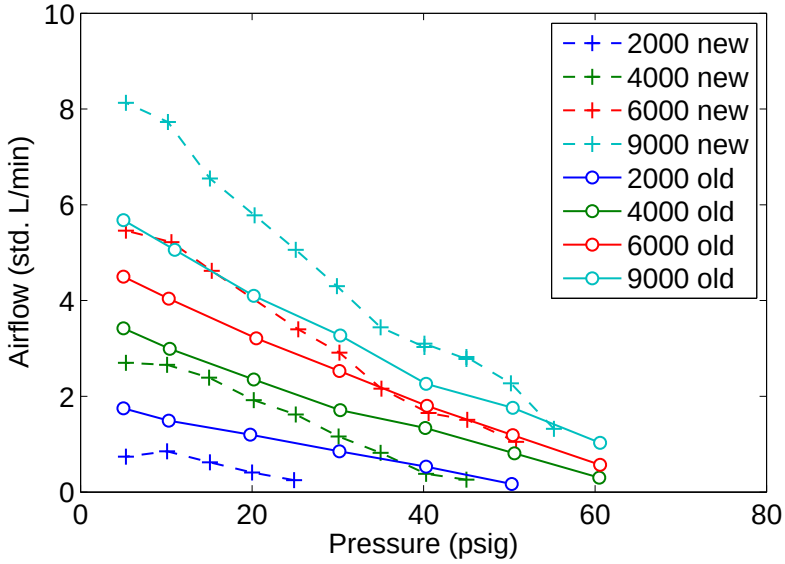

Figure 4.5: Measured airflow with new piston and cylinder compared with previous airflow data for the same speeds

compressor test stand did not differ from expectations. The compressor produced more airflow when running at higher speed because it completes more cycles in a given amount of time. Airflow decreased when the compressor worked against higher backpressure. When the reservoir pressure was higher, a larger portion of the compressor's stroke was used for compression and less for delivery, thus decreasing the volumetric efficiency. At high enough pressure airflow goes to zero as all air in the cylinder is either compressed into the clearance volume or leaked. The maximum output power peaks at a relatively low pressure. A pressure output of 790 kPa (100 psig) is desired to power the pneumatic ankle foot orthosis. In order to achieve this, blow-by leakage will need to be greatly reduced by creating a better seal. It was shown that significant improvement is gained from using oil to help seal the piston/cylinder gap. Also, the geometry of the compressor can be modified. Decreasing the clearance volume at the end of the stroke will allow for higher output pressure and greater volumetric efficiency. The characteristics of the air compressor are examined further in Chapter 5 through quantitative modeling.

Chapter 5

Modeling of the Air Compressor

Two models were created to gain a better understanding of the performance of the miniature air compressor in its independent tests. Their results will be useful when making improvements to the compressor by predicting how it will behave differently after new designs are implemented. The models were based on the cylinder geometry of the compressor test stand, which is almost identical to the miniature free-piston compressor. The thermodynamic states of the air in the compressor were considered throughout one complete cycle. In the first of the two models, the cycle was divided into four ideal gas processes. In the second model the First Law of Thermodynamics – conservation of energy – was used with the entire cycle divided into small, finite steps. One air compressor cycle corresponds to one rotation of the crankshaft in the test stand.

5.1 Four Step Model

The cycle of a reciprocating air compressor can be divided into four parts: compression, delivery, expansion, and intake. The four step model treats these as separate consecutive processes. Figure 5.1 illustrates the four states which are modeled at the beginning of each process. Beginning at the bottom dead center (BDC) position – the end of the

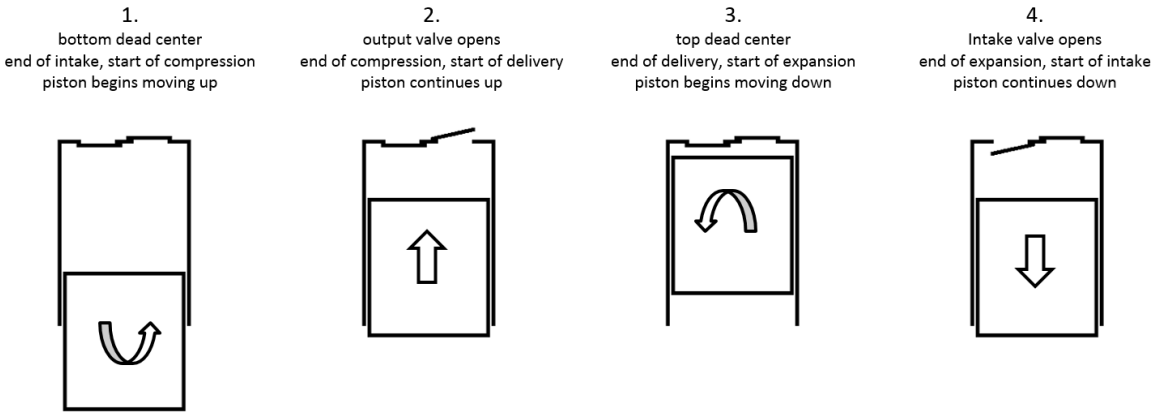

Figure 5.1: The four modeled states of the compressor cycle

intake stroke – the ideal gas conditions at state 1 are set as

$$p_1 = p_{amb} \tag{5.1}$$

$$T_1 = T_{amb} \tag{5.2}$$

$$V_1 = V_{total} = V_c + V_d \tag{5.3}$$

where V_c is the clearance volume and V_d is the displacement volume of the compressor. Pressure and temperature are set at ambient conditions, and volume is equal to the total contained volume of the cylinder. A purely adiabatic process is assumed as the air is compressed to the reservoir pressure, p_{res}. State 2 is the condition where the output valve opens

$$p_2 = p_{res} \tag{5.4}$$

$$T_2 = T_1 \left(\frac{p_2}{p_1}\right)^{\frac{\gamma-1}{\gamma}} \tag{5.5}$$

$$V_2 = V_1 \left(\frac{p_1}{p_2}\right)^{\frac{1}{\gamma}}. \tag{5.6}$$

Air is pushed out of the compressor to the reservoir through the delivery phase, reaching state 3. The state of the gas is unchanged, so the pressure and temperature are equal to state 2 when the output valve closes at top dead center (TDC). The volume at state

3 is equal to the clearance volume of the compressor, which was measured from the test stand. The state 3 conditions are

$$p_3 = p_2 \tag{5.7}$$

$$T_3 = T_2 \tag{5.8}$$

$$V_3 = V_c \ . \tag{5.9}$$

Then the pressurized air left in the clearance volume expands as the piston moves down. Adiabatic expansion from state 3 to ambient pressure gives state 4, the condition where the intake valve opens. The pressure at state 4 is equal to ambient pressure, and the temperature and volume are calculated as

$$p_4 = p_1 = p_{amb} \tag{5.10}$$

$$T_4 = T_3 \left(\frac{p_4}{p_3} \right)^{\frac{\gamma - 1}{\gamma}} \tag{5.11}$$

$$V_4 = V_3 \left(\frac{p_3}{p_4} \right)^{\frac{1}{\gamma}} . \tag{5.12}$$

The intake process leads back to state 1 and the cycle is complete. There is no change to the thermodynamic state of the air during intake. This simple thermodynamic model is an ideal case. Because there are no losses, it ends with $T_4 = T_1$, so mixing does not need to be considered during intake. The input work is calculated for each process as

$$W_{12} = n_1 * c_v * (T_2 - T_1) \tag{5.13}$$

$$W_{23} = (p_2 - p_{amb}) * (V_2 - V_3) \tag{5.14}$$

$$W_{34} = n_3 * c_v * (T_4 - T_3) \tag{5.15}$$

$$W_{41} = (p_{amb} - p_1) * (V_1 - V_4) \ , \tag{5.16}$$

and the sum gives the total work for one cycle. Each of these are plotted in Fig. 5.2 for a range of reservoir pressure (p_2). The net work goes to zero at 750 kPa (94 psig). Above this pressure the volumetric efficiency is zero since the air compressed in the cylinder does not reach a pressure higher than the reservoir to open the output valve. Ideally, all work done to compress the air is recovered from expansion. Figure 5.3 is a plot of the ideal volumetric efficiency. Since this model is ideal, the output work equals

the input work. With the ideal gas law, the moles of air contained at each state are easily calculated. The difference $n_2 - n_3$ is the amount of air delivered to the reservoir in one cycle.

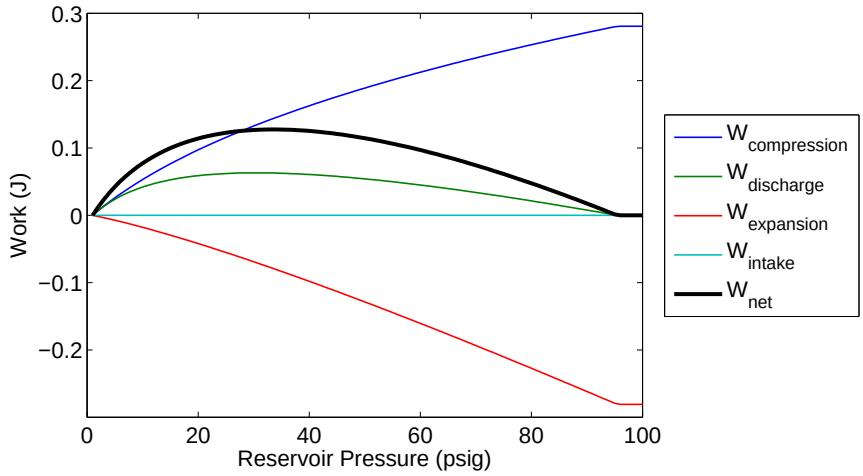

Figure 5.2: Work of each of the four compression processes for a range of pressure p_2

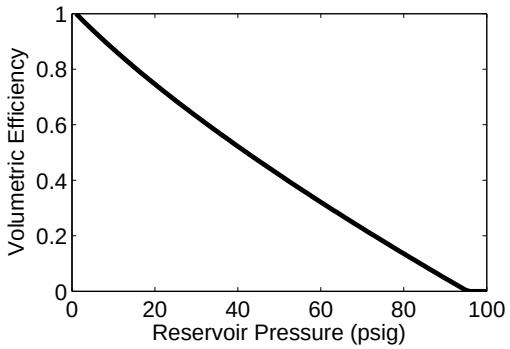

Figure 5.3: Ideal volumetric efficiency

The air compressor has losses which must be considered for the model to be realistic. The two most significant losses are leakage between the piston and cylinder and throttling effects of the compressor reed valves. Pressure differences across the intake and output valves are caused by throttling of the flowing air. No pressure drop was

considered for the air line from the compressor to the reservoir. As a simple approximation, the pressure drop across a valve is proportional to mass flow rate through the valve, or

$$\Delta p = k * \dot{m} \tag{5.17}$$

where k is a constant factor. For simplification Δp is constant throughout the intake and output processes. This model is in terms of moles, n, which is proportional to mass, m, by the molecular mass of air, $M = 28.97$ kg/kmol. In eqn.(5.17), $\dot{m}$ can be replaced using the ideal gas law to give

$$\Delta p = k * M \frac{p\ \dot{V}_d}{R\ T}\ . \tag{5.18}$$

During the delivery or intake process, the volume and mass change proportionally while pressure and temperature are constant. When N is the speed of the compressor in cycles per second and V_d is the displacement volume, the average volume rate of change is

$$\dot{V}_d = V_d * 2N\ . \tag{5.19}$$

Substituting into eqn. (5.18) gives Δp in terms of known values

$$\Delta p = k * M\ \frac{p\ (V_d * 2N)}{R\ T}\ . \tag{5.20}$$

During intake, $\Delta p = p_{amb} - p_1$. Making this substitution, the equation can be solved for

$$p_1 = \frac{p_{amb}}{k * M\ \frac{V_d * 2N}{R\ T_1}\ + 1}\ . \tag{5.21}$$

Similarly during output, $\Delta p = p_2 - p_{res}$. Substituting and solving for p_2 gives

$$p_2 = \frac{p_{res}}{1 - k * M\ \frac{V_d * 2N}{R\ T_2}}\ . \tag{5.22}$$

Implementing these equations in the model accounts for the throttling effect of the valves. The constant values of k can be adjusted to match experimental data. When $k = 0$, $p_1 = p_{amb}$ and $p_2 = p_{res}$, which is the ideal case.

Another loss in the miniature compressor is leakage. This comes from blow-by between the piston and cylinder and poor sealing of the reed valves. A linear orifice flow was used to model the leakage,

$$\dot{m} = k_l * \Delta p \tag{5.23}$$

which is the inverse of eqn. (5.17). Any air that leaks out of the compressor is not delivered to the reservoir. In this model the mass of air delivered depends on the difference between the volume at states 2 and 3, V_2 and V_3. Since a certain portion of this air is lost to leakage, the actual delivered air can be found from $V_{2\text{eff}} - V_3$ where $V_{2\text{eff}}$ is an effective volume slightly less than the actual V_2. The amount of air leaked is represented by $\Delta V = V_2 - V_{2\text{eff}}$. As before, $\dot{m} = k_l * \Delta p$ can be rewritten with the ideal gas law to give

$$M \; \frac{p \; \dot{V}_l}{R \; T} \frac{1}{k_l} = \Delta p \; . \tag{5.24}$$

Pressure and temperature are constant from state 2 to state 3, so p_2 and T_2 are used. Solving for the rate of volume change gives

$$\dot{V}_l = k_l \; \frac{\Delta p \; R \; T_2}{p_2 \; M} \; . \tag{5.25}$$

A finite volume difference is given by

$$\Delta V = \dot{V}_l * t \tag{5.26}$$

where

$$t = \frac{1}{2 \; N} * \frac{V_2 - V_3}{V_d} \tag{5.27}$$

is the approximate time it takes to go from state 2 to state 3. Substituting eqn. (5.25) and eqn. (5.27) into eqn. (5.26) gives

$$\Delta V = \dot{V}_l * t = k_l \; \frac{\Delta p \; R \; T_2}{p_2 \; M} \; \frac{1}{2 \; N} \frac{V_2 - V_3}{V_d} \; . \tag{5.28}$$

Using $\Delta p = p_2 - p_{amb}$ a final simplification gives

$$\Delta V = k_l \left(1 - \frac{p_{amb}}{p_2} \right) \frac{R \; T_2}{M} \frac{V_2 - V_3}{2 \; N \; V_d} \; . \tag{5.29}$$

Because $V_{2\text{eff}} = V_2 - \Delta V$, the following mole counts can be calculated

$$n_{2\text{eff}} = \frac{p_2 \; V_{2\text{eff}}}{R \; T_2} \tag{5.30}$$

$$n_{leaked} = \frac{p_2 \; \Delta V}{R \; T_2} \tag{5.31}$$

$$n_{delivered} = n_{2\text{eff}} - n_3 \; . \tag{5.32}$$

A significant portion of leakage happens during the compression stroke. It changes state 2 by requiring the volume to be further reduced before pressure increases enough to open the output valve. Another ΔV factor was included to account for the air lost during compression. It is calculated similarly to ΔV for delivery, but uses an average temperature and pressure during the compression process. This value is deducted from V_2 to get the actual V_2. This loss may cause the pressure to be reduced such that the output valve will not open, in which case a condition was included to make sure V_2 cannot be less than the clearance volume.

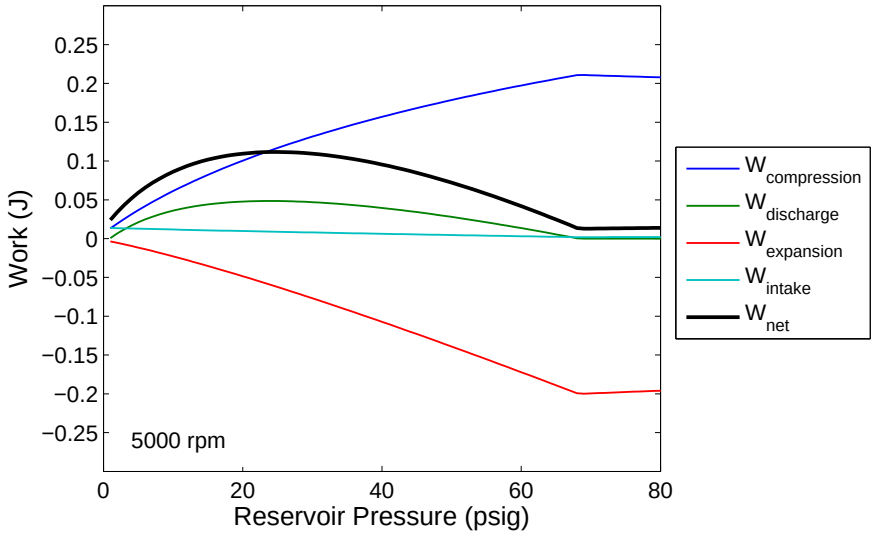

Figure 5.4: Work required for each of the four compression process considering losses

The input power is still calculated the same as before. The required input work of each process is plotted in Fig. 5.4 for a range of pressures at a compressor speed of 5000 rpm. Due to losses, the compressor cannot reach as high of output pressure and the net input work remains above zero at high pressure when there is no output. With losses included, the output power is no longer equal to the input. The output work for each

process is calculated as

$$W_{12} = n_{delivered} * c_v * (T_2 - T_1) \tag{5.33}$$

$$W_{23} = (p_{res} - p_{amb}) * (V_{2\text{eff}} - V_3) \tag{5.34}$$

$$W_{34} = 0 \tag{5.35}$$

$$W_{41} = 0 \ . \tag{5.36}$$

The sum gives the total work output for one cycle, and multiplying by speed gives the output power of the compressed air. Expansion and intake work are zero because all useful output work is from compression and delivery. If losses are set to zero, the total output work equals the input work.

With a known flow rate and temperature, useful power of the compressed air can be found the same way as from experimental data:

$$P = n * N * c_p * T \left[1 - \left(\frac{p_{amb}}{p_{res}} \right)^{\frac{\gamma-1}{\gamma}} \right] . \tag{5.37}$$

This is the same as eqn. (4.3), but the molar flow rate is represented by $\dot{n} = n * N$ where N is the speed of the compressor in cycles per second. If the compressed air can be used at elevated temperature as it exits the compressor, it could provide more power. When the air in the reservoir cools down to ambient temperature, energy is lost. Since the model gives the temperature of the air output from the compressor, this power is known and the cooling loss can be found. At typical operating conditions, it was found that cooling causes about 50% loss in the energy of the air stored in the reservoir.

The model was implemented in Matlab and its parameters were adjusted to match the data from the compressor tests. A constant, k_i, is associated with each of the four loss factors: input valve throttling, output valve throttling, leakage during compression, and leakage during delivery. When all the k's are zero, the model is the ideal case. To reduce the number of parameters, both throttling constants were set equal and both leakage constants were set equal. The two remaining constants were then adjusted until the model's airflow data appeared similar to the experimental data from the compressor test stand. Figure 5.5 shows test data overlaid with results from this model. The model fits the experimental data well except at 7000 rpm. There appears to be a factor that deviates from the model at high speed. Above 550 kPa (65 psig), the modeled airflow

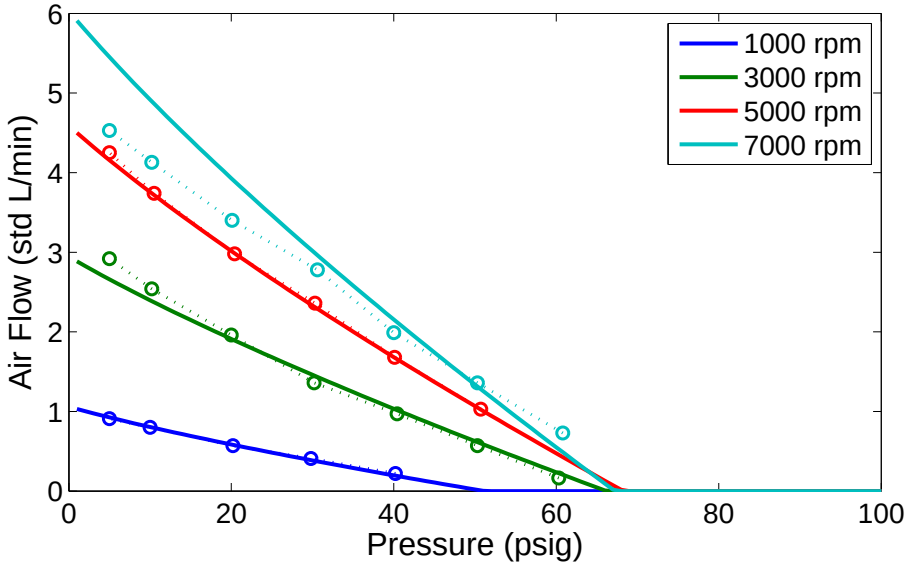

Figure 5.5: Modeled airflow (solid lines) overlaid with experimental data (circles)

for 7000 rpm drops below that of 5000 rpm. This is due to the increased effect of valve throttling at high speed. In the experimental data, the throttling effect appears to be less pronounced as the airflow at 7000 rpm remains above that at 5000 rpm.

After the parameters were adjusted to reflect real conditions, the model's other results were used to predict performance of the compressor. The calculated output power peaks when the reservoir pressure is near 270 kPa (25 psig) (Fig. 5.6). This is the power of the warm air exiting the compressor. After it cools, the available power will be about half. At higher pressure, the power drops off due to the decreased flow rate and goes to zero when volumetric efficiency (Fig. 5.9) goes to zero.

Figure 5.7 shows the overall efficiency of the compressor based on the energy of the warm air exiting the device and Fig. 5.8 shows the efficiency of the system assuming the compressed air will be used after it cools to ambient temperature. Figure 5.7 uses power found from eqns. (5.33) and (5.34), and Fig. 5.8 uses the power calculated in eqn. (5.37) with $T = T_{amb}$. The cooling effect alone cuts the overall efficiency by about half. The efficiency plots are almost flat through most of the pressure range, but drop off at zero pressure and at high pressure when the airflow approaches zero. Without losses or heat transfer, the efficiency would be 1 up to the maximum possible pressure

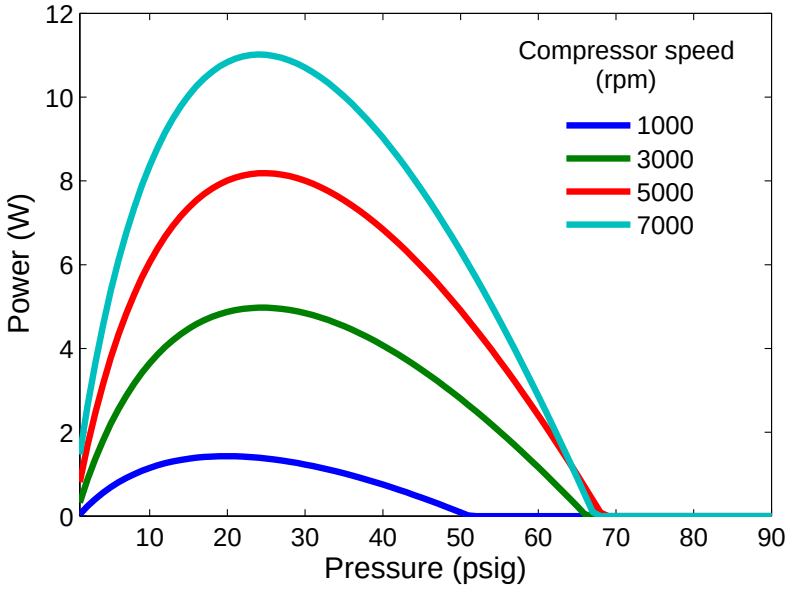

Figure 5.6: Output power prediction of the four step model

where it would drop to zero.

The volumetric efficiency is near one at low pressure and decreases as the pressure increases (Fig. 5.9). Volumetric efficiency drops faster for low compressor speeds as the leakage effect is greater at slow speeds. At low pressure, the losses from throttling have greater effect than leakage. Throttling losses increase and leakage decreases at higher speeds. Therefore, the slower compressor speeds have higher volumetric efficiency near zero reservoir pressure, but the faster speeds are more efficient at higher pressure. The maximum achievable pressure depends on leakage. At higher speed, flow can be achieved at higher pressure due to less leakage. The experimental volumetric efficiency is overlaid in Fig. 5.9. The model matches better for moderate speeds of 3000 and 5000 rpm than it does at the lowest and highest speeds.

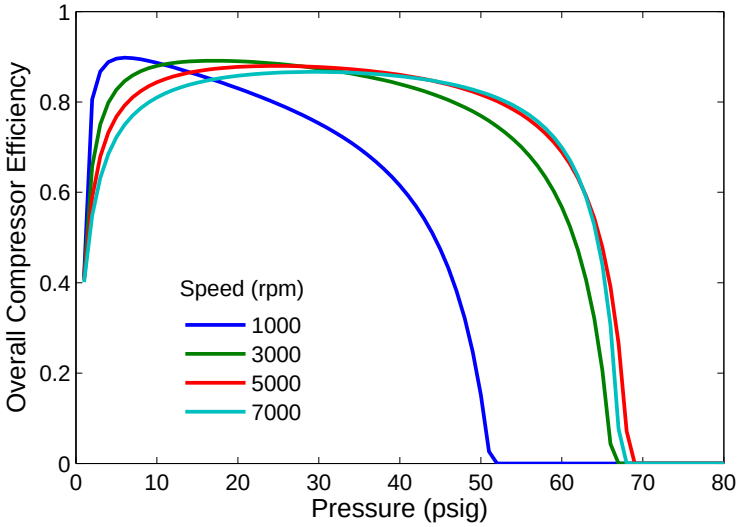

Figure 5.7: Overall efficiency prediction of the four step compressor model

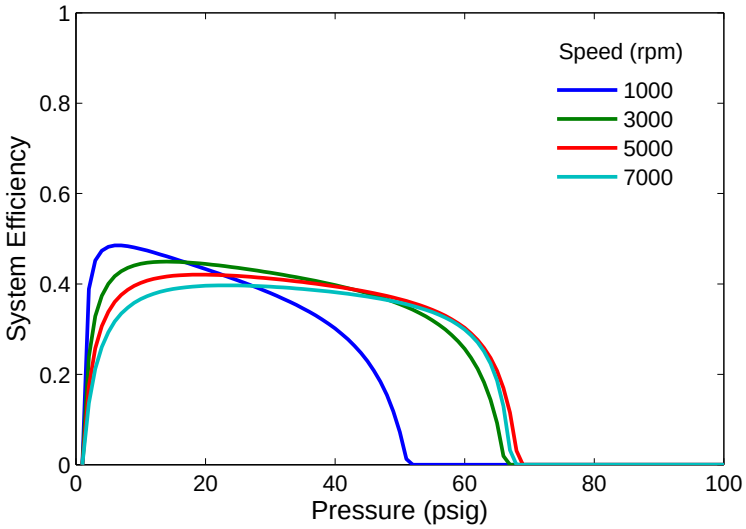

Figure 5.8: Overall system efficiency including cooling effects

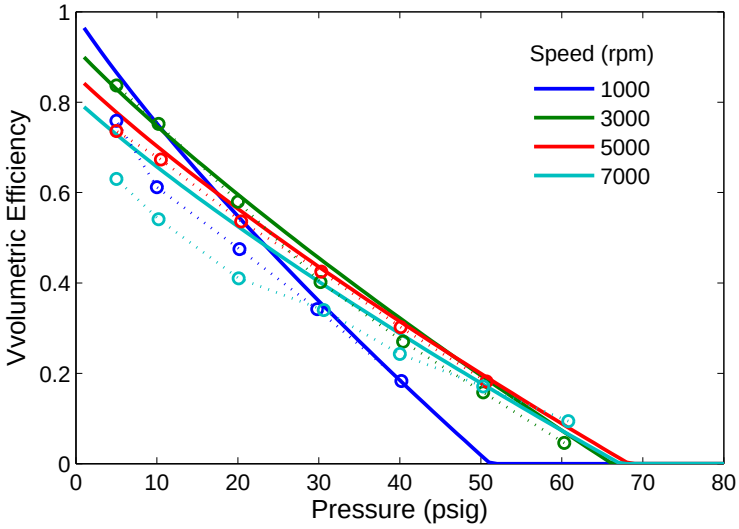

Figure 5.9: Volumetric efficiency of the compressor as predicted by the four step model (solid lines) overlaid with experimental data (circles)

5.2 Iterative Model

To gain more realism in the model, the thermodynamic state should be calculated continuously throughout the cycle instead of at only four discrete points. A new model was created for this reason. It was based on the program Aircycle [25], which models internal combustion piston engines iteratively throughout the cycle. This model considers the volume of the cylinder to be an open system. The thermodynamic states are calculated based on conservation of energy.

Heat transfer was neglected in this model. The highest temperature reached in the ideal four-step model was just over 500 K. At this condition, the maximum heat transfer to the cylinder walls through convection, assuming a Nusselt number of 4 in the cylinder, was 0.7 W. The temperature was this high for only a short part of the cycle, and losses reduce the maximum temperature even further. Throughout most of the cycle when the temperature of the air is lower, the heat transfer rate will be less. Therefore, a reasonably accurate model can be created with the assumption that there is no heat transfer.

One cycle of the air compressor is completed with one rotation of the crankshaft. It was broken down into 720 half-degree intervals. Since the crankshaft is run at constant speed by a motor, crankshaft angle is the input to the system. This directly corresponds via slider-crank mechanics to the piston position at every point in the cycle, which gives the volume based on the geometry of the compressor. The cycle could be broken into more parts with smaller step size, but it was found that the results did not change significantly beyond half-degree intervals. Also, a higher number of points would increase the computational power required.

The volume for every half-degree position is calculated based on crank and slider motion. Cylinder volume is input to the model at each step, and pressure, temperature, and mass are calculated from an energy balance. The mass lost in each step due to leakage is

$$\Delta m_{leak} = \dot{m}t \tag{5.38}$$

where $t = \frac{rpm}{(720*60)}$ is the time step. The leakage rate $\dot{m}$ was found as explained in the following subsections.

The reed valves of the compressor were modeled as simple springs. The valve lift is

proportional to the force caused by a pressure differential. When a pressure difference exists to push the valve open, the orifice flow through the valve depends on the area, which is proportional to the valve lift. A typical orifice flow model was used for the air moving through either the intake or output valves,

$$\dot{m} = A * C_d \sqrt{\frac{p\ M}{T\ R}\ \Delta p} \tag{5.39}$$

where A is the area and

$$\Delta p = \begin{cases} p_{amb} - p & \text{intake} \\ p - p_{res} & \text{output .} \end{cases} \tag{5.40}$$

This model of the valves is more realistic than simply fully opened or closed positions, as was used in the first model. Throttling effects are automatically included in the orifice flow calculations due to the variable valve area. The adjustable parameters are the spring constant for each valve and the flow coefficient, C_d.

Conservation of energy was applied based on Aircycle [25]. Kinetic and potential energy are ignored leaving just internal energy,

$$\Delta U = \Sigma Q + W + \Sigma\ h_i * m_i\ . \tag{5.41}$$

Since heat transfer is neglected in this model, Q is set to zero. The thermodynamic work is

$$W = p\Delta V. \tag{5.42}$$

The energy entering or exiting the system with the flowing mass is

$$\Sigma\ h_i * m_i = \Sigma\ \Delta m * T * c_p\ . \tag{5.43}$$

Three $h_i * m_i$ terms in eqn. (5.41) account for air intake, output, and leakage. Air exiting the compressor is at the temperature of the system and that entering is at ambient temperature. The conservation of energy equation can be solved to get the change in temperature:

$$\Delta T = \frac{1}{c_v(m + \Delta m_{in} + \Delta m_{out})} \left[Q - W + \Delta m_{in}(T_{amb} c_p - T c_v) + \Delta m_{out} \left(T \frac{R}{M} \right) \right]. \tag{5.44}$$

The new conditions at the end of the step are found by

$$T = T + \Delta T \tag{5.45}$$

$$m = m + \Delta m_{in} + \Delta m_{out} \tag{5.46}$$

$$p = R\frac{T}{V}\frac{m}{M} \ . \tag{5.47}$$

The value of Δm_{in} is always positive corresponding to air entering the cylinder, and the value of Δm_{out} is always negative corresponding to air exiting the cylinder. This produces the next state which will serve as the input for the subsequent step.

The model begins at the bottom dead center position of the cycle, which is the end of intake, so initial conditions are set at ambient pressure and temperature. The initial mass of air in the cylinder is easily found with the ideal gas law. The model runs through eight cycles to reach equilibrium and data from the final cycle are output.

As with the four step model, the iterative model can be verified by adjusting its parameters to match experimental results. Since the iterative model calculates the gas states throughout the compressor cycle, it can be compared directly against the measured cycle pressure of the test compressor. Due to the small scale of the compressor, there was not room to insert a pressure sensor in the cylinder. Therefore, the compressor head containing the valves was removed and replaced with the power head from the engine prototype. A pressure sensor (Optrand, model D22255-P) was used in the power head for measuring cylinder pressure. The physical geometry of the model was updated to reflect the different head. Since there were no input or output valves for this test, all valve flow was eliminated and the model was reduced to have only one parameter, the leakage constant. It was assumed that blow-by leakage between the piston and cylinder behaves the same way regardless of whether or not air is flowing in and out through valves. Once the leakage parameter was set, the valves were added back into the model and the measured airflow data was used to set the valve flow parameters of the model.

5.2.1 Linear Leak Model

The blow-by leakage between the piston and cylinder of the compressor causes significant losses in the system. Therefore, it is important that the leakage be represented accurately in the model. The piston cylinder gap is around 6 μm and its length is about

1 cm. The Reynolds number does not exceeded 1000, so it was assumed that airflow in the gap is laminar. Initially, a linear model was used where the mass flow rate is proportional to the pressure difference

$$\dot{m} = k_l(p - p_{amb}). \tag{5.48}$$

The constant k_l, which includes gap area and flow coefficient, was adjusted so that the modeled pressure matched the experiment throughout the entire cycle. Figure 5.10 shows the first attempt at matching the peak pressure for 5000 rpm. Adjusting k_l moved the peak pressure up and down, but the low pressure consistently was modeled below the actual. Because of this, it was assumed that there is an imbalance between leak into and out of the cylinder. Retaining the linear leak model of eqn. (5.48), separate constants were created for leakage in and out. Now both the high and low pressure during a cycle could be matched to the experiment. This is shown in Fig. 5.11 for 5000 rpm when the constant for leakage in was five times larger than the the constant for leakage out.

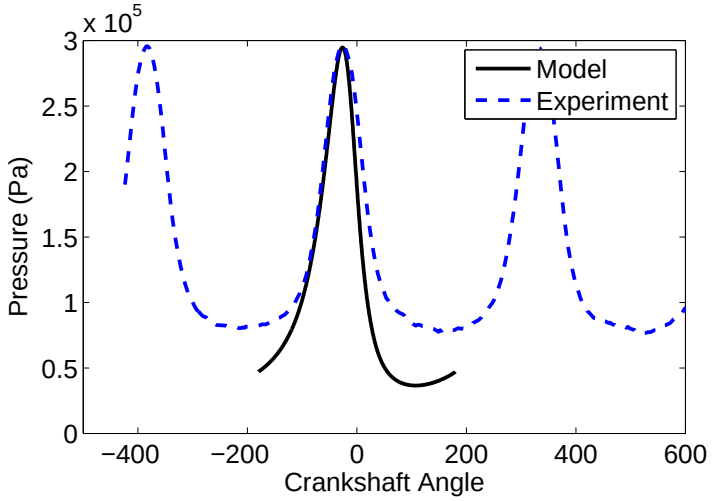

Figure 5.10: The single-coefficient linear leakage model set to match experiment results at 5000 RPM

Due to the relationship of eqn. (5.38), the leaked mass in the model decreases at higher speed because the time step t decreases, leading to higher peak pressure. This was the expected result, as a faster cycle allows less time for air to leak out of the

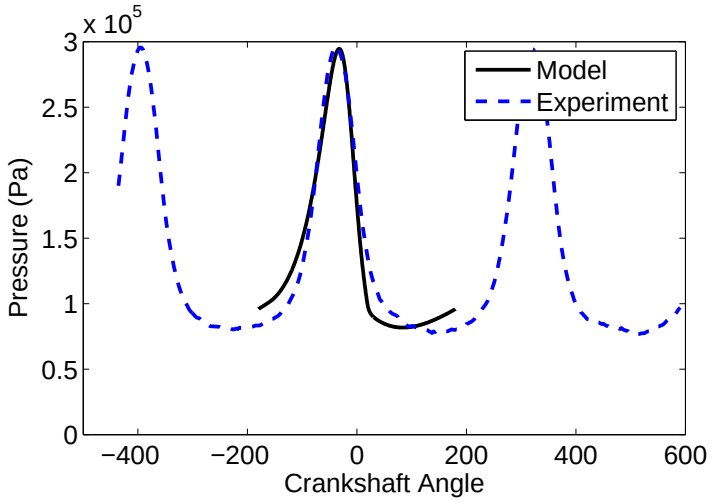

Figure 5.11: The linear leakage model with separate coefficients for in and out set to match experimental data at 5000 RPM

cylinder. The experiment contradicted this. Peak pressure was observed to decrease slightly at higher compressor speed. When the constant leakage parameters $k_{l\ \mathrm{in}}$ and $k_{l\ \mathrm{out}}$ were set for a given speed, they were not accurate for other speeds. Figure 5.12 shows the peak pressure over a range from 1000 to 10,000 rpm. The model data plotted here are based on the linear leakage parameters set to match at 5000 rpm, as in Fig. 5.11. A more complex leak model from Bukac is also shown which will be discussed in the next section. A different set of parameters could be found for each speed, but a more general model is needed that works over all conditions.

The linear leakage model was implemented into the version of the iterative model with the compressor valves. The leakage constants that accurately modeled cycle pressure for 5000 rpm were used, and the model with valves was run. It was expected that the airflow data predicted for 5000 rpm would fit between the experimental data collected at 4000 rpm and 6000 rpm. Figure 5.13 shows that this was not the case. From the experimental data, it appears that the compressor should reach 450-480 kPa (50-55 psig) at 5000 rpm, but the model only reached 270 kPa (25 psig). This model can match the cycle pressure for a given speed, but it over-estimates the leakage, predicting airflow to be much lower than the actual.

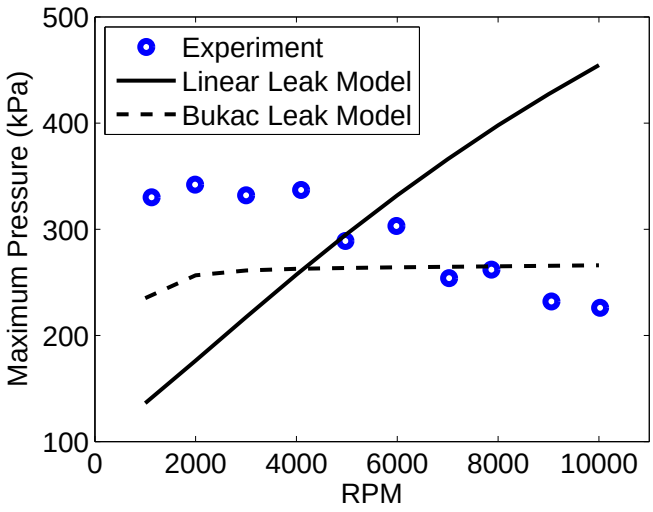

Figure 5.12: Peak pressure during a cycle with no valve flow over a range of speeds

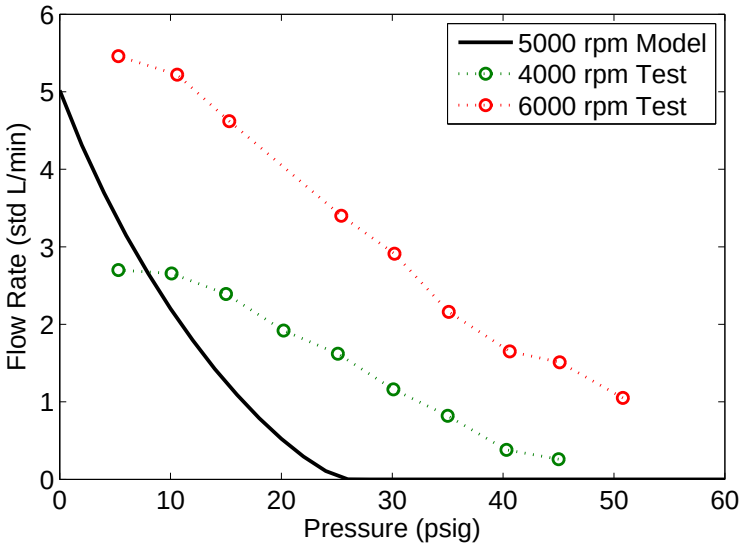

Figure 5.13: Airflow predicted by the iterative model at 5000 RPM when the linear leak model matches cycle pressure as in Fig. 5.11.

5.2.2 Other Leak Models

Since the linear leak model is not accurate, other models were examined. For a model to be general it should not predict higher peak pressure at higher speeds. A standard orifice flow, when implemented, gave similar results to the linear model. Tian laid out a leakage model in his PhD thesis [2]. When implemented, the results did not vary much from the standard orifice, as it still predicted increasing peak pressure with speed. Sher, *et al.* gives a detailed model based on Navier-Stokes equations for blow-by leakage in a miniature engine [26]. The full model only works for high pressure differences like those found in an engine with combustion. However, a simplified version was implemented for the compressor and still predicted increased peak pressure with speed.

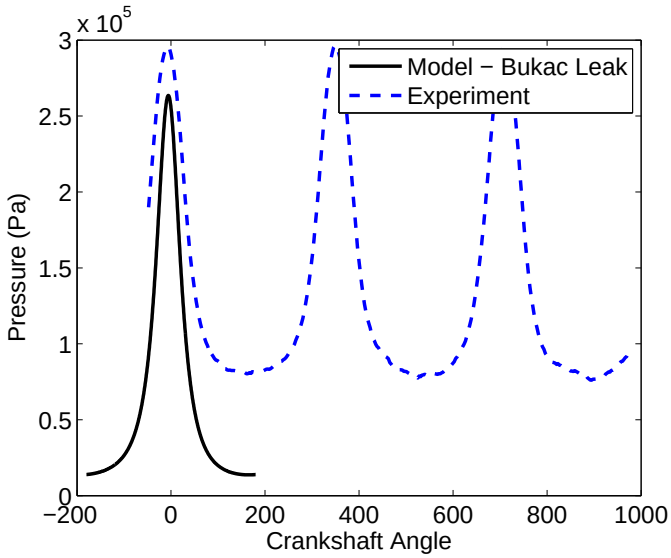

Figure 5.14: Cycle pressure at 5000 RPM when the Bukac leak model is used

Bukac gives a leakage model specifically for reciprocating piston compressors [27]. The model does not have a coefficient to adjust to match experimental data. Initially it predicted the leakage to be much less than the experiment, thus exaggerating expected airflow. A coefficient was added to the model to scale the leaked mass throughout the cycle. With the coefficient set to 100 and the piston cylinder gap set at 7 μm, the model approached the experimental data. With Bukac's leakage model, peak pressure is relatively level versus speed compared with other models (see Fig. 5.12). Over

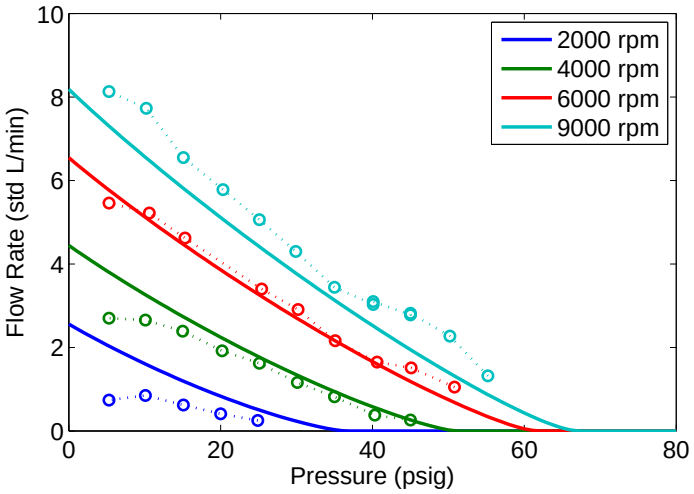

Figure 5.15: The airflow model prediction using Bukac leakage (solid lines) compared to experimental data (circles)

the modeled speed range of 1000 to 10,000 rpm, it gave peak pressure no more than +100/−50 kPa from the experimental peak pressure. The minimum cycle pressure, however, was almost 70 kPa below the experimental minimum pressure. Setting different constant parameters for leak in and leak out did not change the minimum pressure with the Bukac model. Figure 5.14 compares the experimental cycle pressure with that of the iterative model using Bukac's leakage model. This does not match as well as expected, but it is close enough to result in reasonable predictions of airflow in the full model. The pressure sensor used for measuring cycle pressure is well suited for engine cylinders and is more accurate at higher pressure. In these tests, the cylinder pressure is below ambient for part of the cycle, and the sensor may not be as accurate at low pressure. This may be part of the reason the model does not match the reported test data through the low pressure portion of the cycle.

When valve flow was incorporated with this leakage model, the airflow came closer to matching the experiment (Fig. 5.15). The output power of the air after cooling in the reservoir is plotted in Fig. 5.16. The model makes a good prediction of power in the operational range near 6000 rpm, but is less accurate at higher and lower speed. Figure 5.17 shows the predicted volumetric efficiency overlaid with experimental data. This was not predicted as accurately by the model; error is larger at low speed.

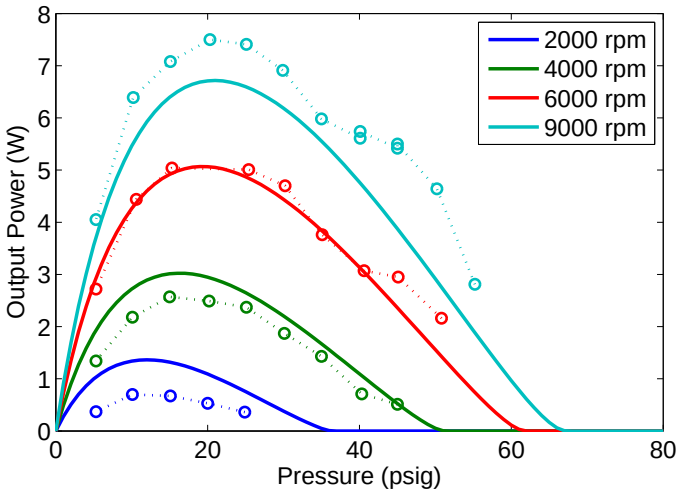

Figure 5.16: The output power of cool air predicted by the model using Bukac leakage (solid lines) compared to calculated power output of the experiment (circles)

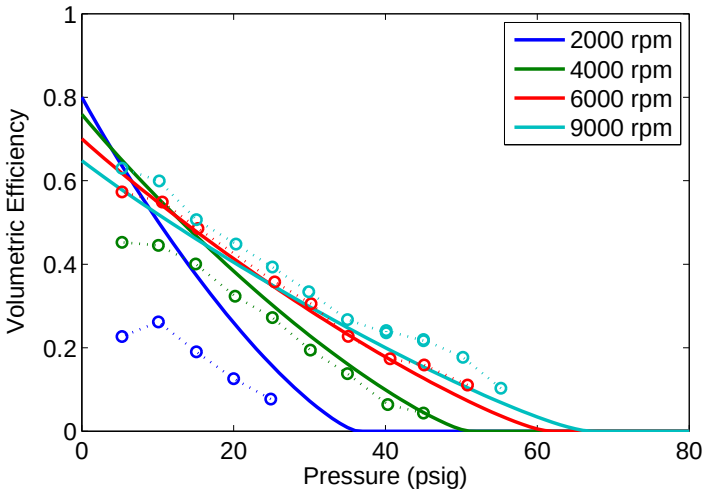

Figure 5.17: The volumetric efficiency predicted by the model using Bukac leakage (solid lines) compared to the experimental volumetric efficiency (circles)

5.3 Conclusions from Compressor Modeling

The miniature air compressor was modeled to gain a better understanding of the thermodynamics in the device and to predict performance after future design changes.

The four step model matched the experimental data well considering its simplicity. It was useful for general predictions of airflow, power, and efficiency. After realizing the complexity of the leakage phenomenon, it is curious why this model worked so well. It does not predict properties of the air in the cylinder throughout the compressor cycle, where the error in leakage calculations is most noticeable.

The iterative model was created to gain a more detailed understanding of the compressor by modeling the entire cycle instead of just four states. To verify this model against experimental results, slight changes were made to the test stand to isolate the blow-by leakage. It was found that peak pressure of the cycle did not depend strongly on compressor speed, which was unexpected. The leakage was more complex than expected and proved difficult to model accurately. Modeling the leakage as an orifice flow did not work. The leakage model from Bukac came closer to matching the experiment when a constant parameter was added. The iterative model predicts output airflow and power reasonably well while approximating cycle pressure. The error in matching cycle pressure, especially below ambient, could have been caused by error in the experimental data from the pressure sensor. The Bukac model was the best of the leakage models that were used, but more detailed leakage model may lead to even more accurate results from the iterative compressor model. In order to gain even more realism and higher precision throughout the cycle, a consideration for heat transfer could be included.

It was found that the heat lost from the compressed air in the reservoir reduced available power by half. Therefore, in the design of a pneumatic power supply, efficiency will be gained by not allowing the pressurized air to cool before it is used. Cooling can be reduced by insulating the reservoir and minimizing the length of the air lines. A smaller reservoir will allow the warm air to be used sooner after it is compressed, but it will cause the engine compressor to cycle on and off more often.

Chapter 6

Conclusions

Limited runtime is the biggest challenge for the miniature engine compressor. For an adequate seal with low friction, even greater precision is needed than that of the new pistons and cylinder liners that were fabricated and tested. It is likely that thermal expansion plays a role in the piston/cylinder fit; however, it is a secondary issue to the leakage and friction. The engine will not heat up to cause expansion until it starts and runs. Another secondary problem is creating a consistent fuel mixture and scavenging, as this made the engine difficult to start. It was shown that forced air induction did not prevent the engine from stalling. Problems with glow ignition do not need to be addressed if the engine is converted to true homogeneous charge compression ignition (HCCI) because the current ignition system would be eliminated. A simple attempt to run in HCCI mode was made. The glow plug was eliminated and model airplane diesel fuel was used. Although the engine was heated to aid compression ignition, the effective compression ratio was not high enough to ignite the mixture. Once a good seal is achieved between the piston and cylinder, HCCI operation should be possible.

When the free-piston prototype ran for short periods of time, the compressor output 11 W of power. This is 55% of the goal for the final device. However, efficiency was still much lower than desired, mostly due to the slow and incomplete combustion caused by glow ignition. When true HCCI is successfully implemented, cycle efficiency is expected to greatly increase. Efficiency will also be gained by reducing leakage losses in both the engine and compressor as well as lessening friction.

The compressor part of the prototype device was tested separately on a test stand.

Operating it continuously provided for more thorough performance measurements than the unreliable free-piston engine. The airflow it produced behaved as expected – it increased with compressor speed and decreased when working against greater backpressure. The compressor can only reach 550 kPa (65 psig), which is less than the 790 (100 psig) desired to power pneumatic devices. This could be improved by reducing leakage losses and reducing clearance volume in the compressor. It was shown that an oil film between the piston and cylinder helps seal the gap and improves performance.

Two models of the miniature compressor were created. Both of them factor in losses due to blow-by leakage and valve throttling. The four-step model is a simplification of the compressor processes. It matched the experimental data reasonably well considering its simplicity. It is useful for general predictions of the airflow, power output and input, and efficiency of the compressor over a range of speed and backpressure. However, the four step model does not give information about every point throughout the cycle. The iterative model calculates the thermodynamic state of the air throughout the entire compressor cycle. It was created to be more accurate than the four-step model. The model does not compute blow-by leakage correctly which prevents it from being as accurate as desired. When the leakage is represented correctly, the iterative model will closely match experimental results. The Bukac leak model appeared to be the best of the leak models examined in this work, but an even more detailed leakage model is needed to reach the desired accuracy. To gain even more accuracy, a representation of heat transfer can be added.

Chapter 7

Recommended Further Work

The primary obstacle is the reliability of the engine. This will be overcome through hardware improvements; some suggestions were made at the end of Chapter 3. More extensive testing is needed to better determine exactly what causes the engine to stall. It would be beneficial to learn what changes as the engine runs. Analyzing emissions will provide details about combustion. As the engine warms up, it would be helpful to know the extent of thermal expansion and what effect it has on the piston/cylinder fit. A method for measuring this in the engine will need to be created.

The variability of the fuel-air mixture provided by the carburetor makes for unpredictable engine starting and may contribute to stalling. This variable could be eliminated from testing by providing pre-mixed fuel and air to the intake, ensuring a consistent, ideal ratio. If this improves reliability, a better fuel metering system needs to be developed for the engine. The prototype should be run with different fuels and a comparison made to determine what works best. An ideal fuel for this device is one that works with HCCI, is clean burning, and is nontoxic. Dimethyl ether is one such fuel.

Running a conventional model airplane engine could still be useful for gaining insight about how the free-piston prototype engine operates. HCCI could be attempted in a model engine first. However, the challenges of ignition timing would need to be dealt with when using a crankshaft engine, since it does not have the variable compression ratio of the free-piston engine.

The air compressor was tested as described in Chapter 4. These tests can be repeated after design changes are made to measure the performance improvement of the compressor. A good seal is important for optimal compressor operation. Minimizing the friction between the piston and cylinder will also increase efficiency. These factors should be easier to address in the compressor because the components do not need to withstand the heat of combustion and associated thermal expansion. Piston rings or O-rings made from a low-friction polymer such as PTFE are possible. To avoid the small scale complexity of creating rings, making the piston with a low-friction polymer may be adequate.

The compressor models can be used predict how physical changes to the air compressor will affect its performance. The iterative model will be most valuable if it is first improved to be more accurate. Finding a better leak model and implementing a consideration for heat transfer will help with this. The current iterative model uses first order calculations, but a higher order model, such as Runge-Kutta, could be explored to add more detail.

References

[1] K. Alex Shorter, F. Geza Kogler, Eric Loth, William K. Durfee, and Elizabeth T. Hsio-Wecksler. A portable powered ankle-foot orthosis for rehabilitation. *Journal of Rehabilitation Research & Development*, 48(4):459–472, 2011.

[2] Lei Tian. *Miniature Homogeneous Charge Compression Ignition Free-Piston Engine Comperssor*. PhD thesis, University of Minnesota, June 2013.

[3] Lei Tian, David B. Kittelson, and William K. Durfee. Miniature hcci free-piston engine comperssor for orthosis application. *SAE International*, 2009. SAE #2009-32-0176.

[4] Hans T. Aichlmayr. *Design Considerations, Modeling, and Analysis of Micro-Homogeneous Charge Compression Ignition Combustion Free-Piston Engines*. PhD thesis, University of Minnesota, December 2002.

[5] R. Mikalsen and A.Pl Rolkilly. A review of free-piston engine history and applications. *Applied Thermal Engineering*, 27:2339–2352, October 2007.

[6] Vittorio Manente, Per Tunestal, and Johansson Bengt. Mini high speed hcci engine fueled with ether: Load range, emissions characteristics and optical analysis. *SAE International*, 2007. SAE #2007-01-3606.

[7] Vittorio Manente, Per Tunestal, and Johansson Bengt. Influence of the wall temperature and combustion chamber geometry on the performance and emissions of a mini hcci engine fueled with diethyl ether. *SAE International*, 2008. SAE #2008-01-0008.

[8] Kyle Collair and Gareth Floweday. Understanding hcci characteristics in minni hcci engines. *SAE International*, 2008. SAE #2008-10-1662.

[9] Kurt D. Annen, David B. Stickler, and Jim Woodroffe. Miniature internal combustion engine-generator for high energy density portable power. In *26th Army Science Conference*, December 2008. Aerodyne Research, Inc.

[10] James P. Szybist and Bruce G. Bunting. The effects of fuel composition and compression ratio on thermal efficiency in an hcci engine. *SAE*, 2007. SAE #2007-01-0476.

[11] Kathi Epping, Salvador Aceves, Richard Bechtold, and John Dec. The potential of hcci combustion for high efficiency and low emissions. *SAE*, 2002. SAE #2002-01-1923.

[12] Anders Hultqvist, Ulf Engdar, Bengt Johansson, and Jens Klingman. Reacting boundary layers in a homogeneous charge compression ignition (hcci) engine. *SAE International*, 2001. SAE #2001-01-1032.

[13] Kim R. Hansen, Jakob D. Dolriis, Christoffer Hansson, Claus S. Nielsen, Spencer C. Sorenson, and Jesper Schramm. Optimmizing the performance of a 50cc compression ignition two-stroke engine operating on dimethyl ether. *SAE International*, 2011. SAE #2011-01-0144.

[14] Robert R. Raine and Harald Thorwarth. Performance and combustion characteristics of a glow-ignition two stroke engine. *SAE International*, 2004. SAE #2004-01-1407.

[15] H.T. Aichlmayr, D.B. Kittelson, and M.R. Zachariah. Micro-hcci combustion: Experimental characterization and development of a detailed chemical kinetic model with coupled piston motion. *Combustion and Flame*, 2003.

[16] G.K. Aue. Piston ring scuffing-general review. In *Proceeding of Conference Sponsored by the Tribology Group, the Combustion Engines Group, and the Automobile Division of the Institution of Mechanical Engineers*, pages 1–7, 1975.

[17] R Munro. Diesel engine ring scuff-is there a major problem? In *Conference on Piston Ring Scuffing, The Institution of Mechanical Engineers, London*, 1975.

[18] Kevin C. Radil. The influence of honing on the wear of ceramic coated piston rings and cylinder liners. Technical report, U.S. Army Vehicle Technology Directorate, National Aeronautics and Space Administration, Glenn Research Center, Cleveland, Ohio 44135, February 2000.

[19] T.S. Eyre and K.K. Dutta. Some metallurgical aspects of scuffing. Brunel University, Uxbridge, Middlesex.

[20] Ka Jun Ng, Farhad B. Bahaaideen, Horizon Gitano-Briggs, and Zaidi Mohd Ripin. Friction and wear characteristics of tic surface coatings in a small two-stroke utility engine. *SAE International*, 2008. SAE #2008-32-0006, JSAE #20084706.

[21] E.J. Murray. A survey of scuffing in spark ignition engines.

[22] Guido Keijzers. Thermal spray coatings and high performance engine valves. *Advanced Materials & Processes*, 168(8):42, August 2010. 52643386.

[23] Juliano Araujo and Robert R. Banfield. Dlc as a low friction coating for engine components. *SAE International*, 2012. SAE # 2012-36-0255, SAE Brasil.

[24] Oki Sato, Masaaki Takiguchi, Takayuki Aihara, Yulchi Seki, Kazuhiro Fujimura, and Yukio Tateishi. Improvement of piston lubrication in a diesel engine by means of cylinder surface roughness. *SAE International*, 2004. SAE #2004-01-0604.

[25] Duane R. Amlee. Aircycle, 1990. University of Minnesota.

[26] I. Sher, D. Levinzon-Sher, and E. Sher. Miniaturization limitations of hcci internal combustion engines. *Applied Thermal Engineering*, 29:400–411, 2009.

[27] H. Bukac. Optimum piston-bore fit for maximum comperssor efficiency. In *Fifteenth Internantional Compressor Engineering Conference*, number 1430, pages 523–530. American Institute of Aeronautics and Astronautics, Purdue e-Pubs, Purdue University, July 2000.

Appendix A

Standard Operation of the Free-Piston Prototype

The prototype device is run in a laboratory in its specially designed test stand. The test stand is mounted on a table and holds the prototype securely during operation. A photograph of the experiment apparatus is shown in Fig. A.1. Data acquisition equipment is used to measure various aspects of operation.

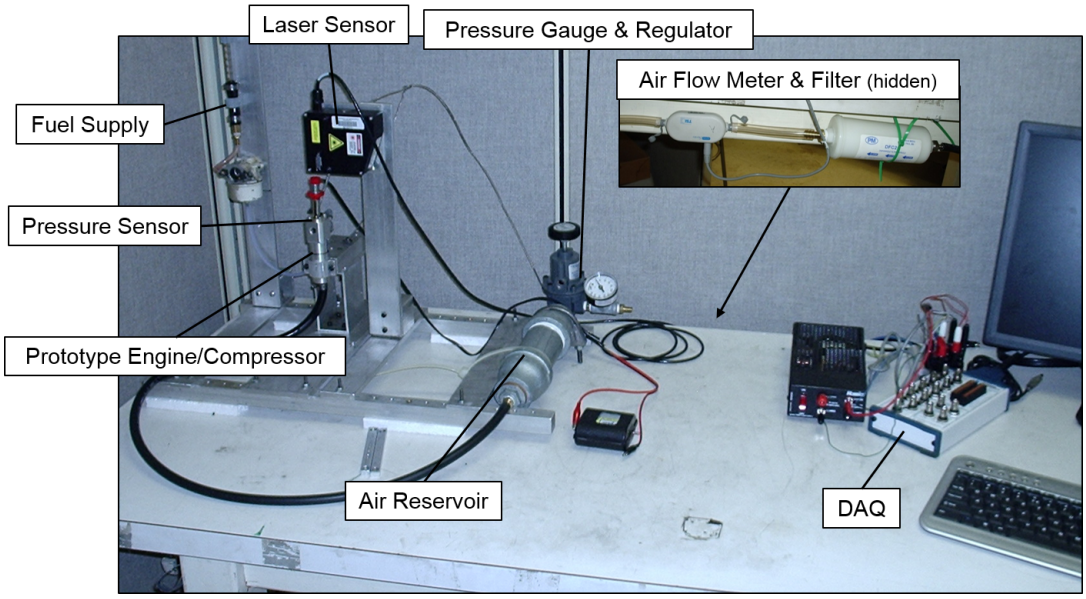

Figure A.1: The prototype test stand and associated data acquisition equipment

Following is a list of the sensors and equipment used to collect data.

- Optrand model D22255-Q pressure sensor measures combustion pressure in the engine cylinder. It is powered with 12 V and outputs a signal in the range 0.5-4.5 V.
- MTI model LTC-120-20-SA laser sensor measures the position of the piston assembly. Powered by 12 V, output 0-5 V.
- Omegadyne model PX309-150G5V pressure sensor measures the air pressure in the reservoir. Powered by 12 V, output 0-5 V.
- TSI model 41221 airflow sensor measures mass flow rate exiting the reservoir through the backpressure regulator. Powered by 5 V, output 0-4 V.
- National Instruments BNC 2110 board for connecting sensor input to the computer.
- National Instruments PCI 6143 card in the computer connects to the BNC 2110
- Labview software is used for monitoring and recording data.

A standard procedure should be followed to start and run the prototype engine. The important points are listed below.

- Fuel may be supplied from a burette to measure usage rate. In this case, it should pass through a float bowl to maintain a steady pressure at the carburetor as the level drops. If fuel is supplied from a tank, the fuel level in the reservoir should be near or slightly above the elevation of the carburetor.
- Mount the engine in the test stand and make sure it is fastened securely. Connect the fuel line to the nipple on the needle valve and purge air from the line. Connect the air hose to the compressor output of the prototype. Make sure the sensors and data collection equipment are turned on.
- Power the glow plug with 1.5 V.

- Open the needle valve 4 full turns. This may vary depending on fuel pressure and fuel composition.
- Cycle the engine a few times moving the starting handles by hand to bring fuel into the cylinder. This is only necessary on the first starting attempt.
- Using a pair of metal bars, pull the starting handles all the way down and quickly release them. The piston, pushed by the spring, should shoot upwards creating compression and leading to ignition. If the engine does not start, repeat.
- If the engine becomes flooded with excess fuel, clamp the fuel line to stop the flow. Then either continue cycling the engine to evaporate the extra fuel, or open the combustion chamber by removing the glow plug and allow time for fuel to evaporate.
- If the engine runs, adjust the needle valve to maintain steady operation. Power may be removed from the glow plug.
- To stop the engine, stop fuel flow by pinching the fuel line or closing the needle valve. If the engine stalls, either restart it or clamp the fuel line to prevent liquid fuel from flowing into the carburetor.

The prototype engine needs to be inspected between each run. There are a number of parts that wear out and must be replaced periodically. The following list covers some of these items.

- Piston and cylinder scuffing and wear – The piston and cylinder liner in the engine may sustain scuff marks during operation which can lead to excessive friction and prevent the engine from running. After many cycles, excessive wear may also be present which could be detrimental to operation. If either of these is seen on the parts, they need to be replaced. The piston and cylinder in the compressor should also be inspected. Although less critical for operation, excessive scuffing or wear should be avoided here, as well.
- Rubber bumper – At the end of the stroke, the piston handles contact two rubber bumpers which are designed to absorb excess energy and prevent damage. When

the engine is running, the rubber deteriorates quickly. When the bumpers are worn out, new ones should be inserted. They are made from 1/8" O.D. 50a rubber rod cut to 0.61" long.

- Rebound spring – The spring in the prototype naturally compresses over time, losing a little force. The spring should be replaced if its relaxed length is less than 1.60". The original length is 1.75".

- Compressor valves – The intake and output reed valves in the compressor experience fatigue wear over time. They do not have a valve stop, so hyperextension adds to fatigue. The valves need to be inspected periodically. If cracking is seen, they should be replaced. Compressor valves in poor shape will not hinder engine operation, but will hurt the efficiency of the air compressor.

- Glow plug – Make sure the glow plug glows orange when connected to 1.5 V of power. It may not get hot enough if there is carbon built up on the plug or if the batteries are weak.

- Generally inspect the body of the engine, the piston connecting rod, and all other components. Take note of any damage or unusual wear and make repairs accordingly.

- When reassembling the engine, add a few drops of oil to the piston for lubrication. Standard model fuel works for this since it has 20% oil; the methanol will quickly evaporate leaving a layer of oil.

Appendix B

Mechanisms for Starting the Free-Piston Engine

To start the free-piston engine, as with any engine, the piston must be cycled manually until combustion occurs. This process is simple in crankshaft engines, as the crankshaft just needs to be rotated to move the pistons. Rotational motion can easily be provided by an electric motor. Free-piston engines do not have any rotating parts, so the starting mechanism must directly reciprocate the piston.

The miniature free-piston prototype is started by hand as described in Section 3.2. A starting mechanism is not necessary for testing, but would be helpful. For this device to be a useful portable power supply, an automatic starting mechanism will be required. There are a few different methods that could provide the reciprocating motion necessary to move the piston and start the engine.

A mechanical mechanism external to the prototype could convert rotational motion into reciprocating motion of the piston assembly. Then the starting power could come from an electric motor. The mechanism cannot be a simple crank, however. The compression stroke of the engine should be driven by the rebound spring so that the piston moves fast enough to cause adequate compression. A crank connected to the piston assembly would restrain this motion. A better mechanism would involve a cam that forces the piston down, compressing the spring, and then releases it to rebound naturally. It may be possible to implement this sort of cam mechanism to operate on

the starting handles of the the current prototype. If a new prototype is designed, it would be easier to integrate a mechanical starting system.

A mechanical starting system would be too cumbersome and add extra weight to the final portable free-piston device. Also, it will be undesirable to carry a second power supply just for starting the engine. In its final form as a portable power supply, the free-piston engine should use compressed air to start. Since the device produces compressed air, there will be no other energy source required. The control system would be designed so that the engine re-starts before the compressed air reservoir is completely empty. The only added weight of an air starting system would be valves and extra air lines. Through the use of automatic valves, compressed air from the reservoir will drive the pistons down. The air will then be released quickly so that the piston rebounds. This process can be repeated rapidly until the engine starts and runs. A compressed air starting system is not practical to implement on the current prototype due to the complexity of the valves and controls. The system can be developed after further research progress on the prototype has been made.

Appendix C

Considerations for Lubrication in the Free-Piston Engine

The use of low-friction polymers in the cylinder or piston of the engine likely will not be possible because of the high temperature of combustion. Some sort of ceramic coating or diamond like carbon might work well. Even with a low-friction material, the presence of oil in the engine will be beneficial. It is known that an oil film between the piston and cylinder helps seal the gap from blow-by leakage. Oils also helps cool two-stroke engines. In order to create a clean operating engine, oil should not be mixed with the fuel. Also, if a gaseous fuel like dimethyl ether is used, mixing oil is not easily done. Because of these reasons, thought has been given to another method for providing oil to the rubbing surfaces in the engine.

It will not be possible to create a system to recirculate oil in the miniature free-piston engine. Without piston rings, the seal will never be good enough to keep the oil contained. However, a dedicated oil system could provide fluid at precisely the correct rate independent of fuel delivery. Oil would be stored in a reservoir and expelled after use. It would either leave with the exhaust, as is typical for two stroke engines, or drain into a catch basin around the engine. If the system is designed precisely, oil will be consumed slowly and there will not be excess to create a mess.

One way to deliver oil to the piston/cylinder interface is through small holes in the cylinder. An example of how this may look is illustrated in Fig. C.1. The size of the

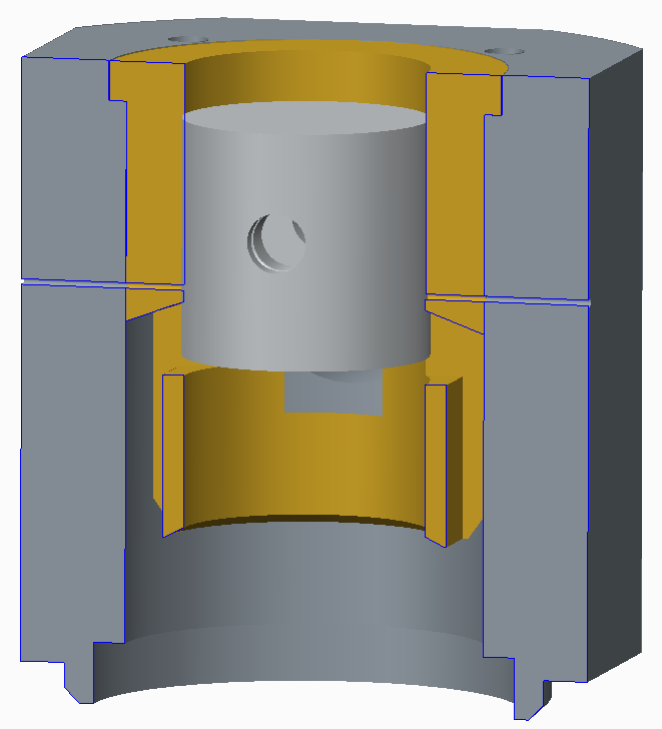

Figure C.1: An illustration of small holes that would deliver oil to the piston.

holes should depend on the viscosity of the oil to be used and the rate it needs to be delivered. The oil will flow through the small holes at ambient pressure due to capillary forces. As the moving piston displaces a small amount of oil, more will be delivered. A series of holes around the piston would be necessary to evenly distribute the oil for lubrication and gap sealing. The vertical location of the holes needs to be optimized. Above the intake ports, as shown in Fig. C.1, is not the best location as elevated pressure from combustion would push the oil back through the conduit. The oil holes must be below the exhaust port so pressure is released before they are exposed. The holes cannot be too low as oil must be spread on the entire piston surface. Maybe the best location would be on the same level as the intake ports. This is something that must be explored when developing the oil system.

This system would be difficult to implement in the current prototype because of the way the cylinder liner fits in the engine block. The oil would need to pass through the block and the liner. It would be difficult to align corresponding holes in the two parts,

and there could be leakage at the interface. Figure C.1 shows the holes in the current engine design, but this is just for illustration purposes. In order to implement this oil system, the engine will need to be re-designed so that the oil holes do not pass through the engine block. This may be done by combining part of the block into the cylinder liner.

Appendix D

Table data in Inches

Cylinder Liners	I.D. (in.)	Pistons	O.D. (in.)	Clearance
Original - stock reamed	0.4927	Stock	0.4923	0.0004
Stock enlarged further	0.4935	Stock with coating	0.4932	0.0003
Custom Fabricated	0.4940	Custom Fabricated	0.4935	0.0005

Table D.1: A reproduction of Tab. 3.1 on p 30. The data are given here in inches for convenience.